Investigation of the effects of nanostructure on the observable behavior of magnetic thin film using large-scale computer simulation

Hong Fu, R. Giles, M. Mansuripur, and G. Patterson

Citation: Computers in Physics **6**, 610 (1992); doi: 10.1063/1.168441
View online: https://doi.org/10.1063/1.168441
View Table of Contents: https://aip.scitation.org/toc/cip/6/6
Published by the American Institute of Physics

Investigation of the effects of nanostructure on the observable behavior of magnetic thin film using large-scale computer simulation

Hong Fu
Optical Sciences Center, University of Arizona, Tucson, Arizona 85721

R. Giles
College of Engineering, Boston University, Boston, Massachusetts 02215

M. Mansuripur
Optical Sciences Center, University of Arizona, Tucson, Arizona 85721

G. Patterson
College of Engineering, Boston University, Boston, Massachusetts 02215

(Received 13 February 1992; accepted 22 April 1992)

Large-scale computer simulations of magneto-optical thin films with nanoscale structures are performed on the Connection Machine. The magneto-optical thin films are modeled by a two-dimensional lattice of magnetic dipoles which follow the Landau–Lifshitz–Gilbert dynamic equation. The effective field on each dipole includes the local anisotropy, the nearest neighbor exchange interactions, the magnetic dipole–dipole interactions, and an externally applied field. The film is divided into many patches (regions) and each patch can have different properties. Four different patchy films are studied. (i) The film has different exchange stiffness constant on the patch borders. (ii) The film has large magnetization, but has zero exchange on the patch borders. (iii) The patches have different easy axis orientations. (iv) The patches have different anisotropy constants. The computer simulations show that films with different kinds of patches have different features in their magnetic behavior. Based on these correspondences between the nanostructure and the magnetic properties, certain features recently observed in several magneto-optical thin films are able to be explained.

INTRODUCTION

The magnetic properties of magnetic thin films depend crucially on the nanostructure that is built in during the film growth processes. A common type of nanostructure is the columnar structure, which is formed due to shadowing of the incident vapor by the growing film. Columnar structures in amorphous RE–TM thin films have been studied by many authors.[1-3] For example, Leamy and Dirks found that the amorphous Gd_xCo_{1-x}, Ho_xCo_{1-x}, Gd_xFe_{1-x}, and Y_xCo_{1-x} $(0.1<x<0.7)$ thin films consists of columns (50–250 Å in diameter) of relatively high atomic density that are separated 10–25 Å apart by a dilute network of atoms.[1] Nanostructure can also occur in amorphous magneto-optical films which do not have columnar structure, but contain occasional crystalline or polycrystalline grains of random size, shape, and orientational packing.[4] These columns or crystalline structures may stem from different seeds, and borders are formed when they merge. Since the exchange interaction of two atoms drops drastically with increasing distance, the exchange couplings between neighboring columns or crystalline structures are expected to be weaker than that for atoms within a column or a crystalline structure. Consequently, the films consist of many loosely connected small regions of different magnetic properties.

The purposes of the present paper is to study how the nanometer scale structures of columnar nature and crystalline grains can affect magnetic properties of the magneto-optical thin films. Although there is little direct information about nanoscale structure and inhomogeneities, their existence is strongly suggested by many observed incoherent and irreversible magnetic processes in magneto-optical thin films, which are at variance with the coherent Stoner–Wohlfarth theory. At this stage, large-scale computer simulations, accompanied by a close comparison with the experiment, become a unique tool for investigating the magneto-optical thin films of nanoscale structure.

The magneto-optical thin films are modeled by a two-dimensional hexagonal lattice with 256×256 dipoles. Each dipole represents a hexagonal slab of the magnetic material with the height of the slab equal to the film thickness h (Ref. 5). The motion of each dipole follows the Landau–Lifshitz–Gilbert equation:

$$\dot{\mathbf{m}} = \gamma \mathbf{m}\times\mathbf{H}_{\text{eff}} + \alpha \mathbf{m}\times\dot{\mathbf{m}}/|m|\,, \tag{1}$$

where $\mathbf{m}$ is the dipole moment at a given site, γ the gyromagnetic ratio, $\mathbf{H}_{\text{eff}}$ the effective field on the site, and α the Gilbert damping constant. Throughout this paper we use $\gamma = -10^7$ Hz Oe^{-1} and $\alpha = 0.5$ (Ref. 6) and the lattice constant $a = 10$ Å in the film plane.[5] The total area of the lattice is thus equal to 0.256×0.222 μm^2. The effective

field $\mathbf{H}_{\text{eff}}$ on each site arises from four sources: the local uniaxial anisotropy, the nearest neighbor exchange, the long-range magnetic dipole–dipole interactions, and an external field. In order to avoid finite-size effect and to use FFT (fast Fourier transformation) in calculating the demagnetizing field, periodic boundary conditions are imposed on the lattice. The details of evaluating the anisotropy, exchange, and demagnetizing fields can be found in Refs. 7–9.

In order to model the effects of nanostructure, the lattice is assumed to consist of many patches (regions) with different properties, e.g., with different easy axis orientations or with different anisotropy constants. The shape and size of each patch are determined by a random process. The stiffness constant A_x, which describe the strength of the exchange interaction, is chosen to be smaller at the patch borders than its value within the patch. Since the patches are weakly coupled to each other, various incoherent and irreversible movements of the dipoles of different patches may occur. The resultant magnetic properties, which are usually measured from various $M-H$ (magnetization versus external field) curves, may depend very much on the assumed patch structures.

The present paper is organized as follows. In Sec. I we discuss how domain wall motion may be affected by the patch borders of weaker stiffness constant. In Sec. II we study the demagnetization of a patchy film which has relatively large saturation magnetization, but has zero exchange on the patch borders. In Sec. III a different mechanism of incoherent magnetization reversal is investigated for a film whose patches have different easy axis orientations. In Sec. IV we assume that the patches all have perpendicular easy axes, but have different anisotropy constant. Some concluding remarks are presented in Sec. V.

In this paper the magnetization state of the film, i.e., the orientations of the dipoles (the magnitude of the dipole moments will not change according to the Landau–Lifshitz–Gilbert equation), is represented by a color code. Since any direction corresponds naturally to a point on a sphere, the orientation of a dipole can be specified by a color according to the following color sphere coding scheme. The color sphere has its equator in the film plane (X-Y plane) and its north and south poles corresponding to the directions ($\pm Z$) perpendicular to the film plane. It is white at its north pole ($+Z$), black at its south pole ($-Z$), and scans the visible spectrum from red ($+X$) through light green ($+Y$), blue ($-X$) to purple ($-Y$) in the manner shown in Fig. 1. Thus the pixel is red when the dipole points along $+X$, blue along $-X$, light green along $+Y$, purple along $-Y$, white along $+Z$, and black along $-Z$. In the same manner, other orientations of the dipole map onto the corresponding color on the color sphere. For example, as the orientation of a dipole moves from the $+X$ direction to the $+Z$ direction in a path on a great circle, the representative color will begin with red for the $+X$ direction, then mixes with decreasing degree of red but increasing degree of white, until it becomes totally white for the $+Z$ direction. Moving toward the $-Z$ direction has the opposite effect, as the color mixes with increasing degree of black. As the only exception of the color coding scheme, we will use grey lines to highlight the patch borders. These grey lines only mark the location of the patch borders; they have nothing to do with the orientation of the dipoles.

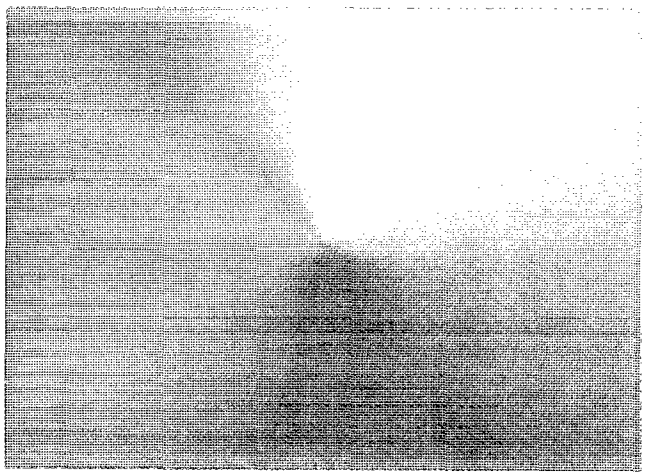

FIG. 1. This color circle is used to encode the direction of a dipole in the plane of the lattice (X-Y plane). In this scheme the red pixel represents the $+X$ direction, light green the $+Y$ direction, blue the $-X$ direction and purple the $-Y$ direction. When a dipole is not completely in the plane of the lattice, but has a perpendicular component along the $+Z$ (or $-Z$) direction, its associated pixel is a mixing of the color of its in-plane component with certain degree of white (or black), depending on the magnitude of the perpendicular component. A dipole fully aligned in the $+Z$ direction is represented by a white pixel, while a dipole in the $-Z$ direction is represented by black.

I. EFFECTS OF PATCH BORDERS ON COERCIVITY

The magnetic coercivity at the nanoscale is a key factor for the domain wall motion and domain reversal. It directly affects the write, erase and overwrite processes on magneto-optical thin films. Recently, Giles and Mansuripur[10] and Mansuripur *et al.*[11] studied the effects of various defects and inhomogeneities on the coercivity using large-scale computer simulations on the Connection Machine. They found, for instance, that voids have insignificant effects on the nucleation coercivity, but that the reverse magnetized seeds of nucleation can substantially reduce the coercivity. In this section we study how the coercivity is influenced by the patch borders with weak exchange.

The patchy film for which the computer simulations were performed is specified as follows. The film thickness $h = 500$ Å, the saturation magnetization $M_s = 100$ emu cm^{-3}, and the anisotropy energy constant $K_1 = 10^6$ erg cm^{-3} (local nominal value) and the exchange stiffness constant $A_x = 10^{-7}$ erg cm^{-1} (nominal value). The film consists of 37 random patches with an average dimension of 400 Å, see Fig. 2. The domain wall width $\pi\sqrt{A_x/\langle K_1\rangle} = 120$ Å, where $\langle K_1\rangle$ is the average anisotropy constant to be discussed below.

The easy axis orientations are set different from site to site. Let $\mathbf{e}_a$ be the unit vector along the easy axis for a given site. It is specified by the spherical angles (θ_a,ϕ_a) in the following way: $\mathbf{e}_a = \sin\theta_a\cos\phi_a\mathbf{e}_x + \sin\theta_a\sin\phi_a\mathbf{e}_y + \cos\theta_a\mathbf{e}_z$, where $\mathbf{e}_x$, $\mathbf{e}_y$, and $\mathbf{e}_z$ are unit vectors along the $+X$, $+Y$, and $+Z$ directions, and θ_a is the angle be-

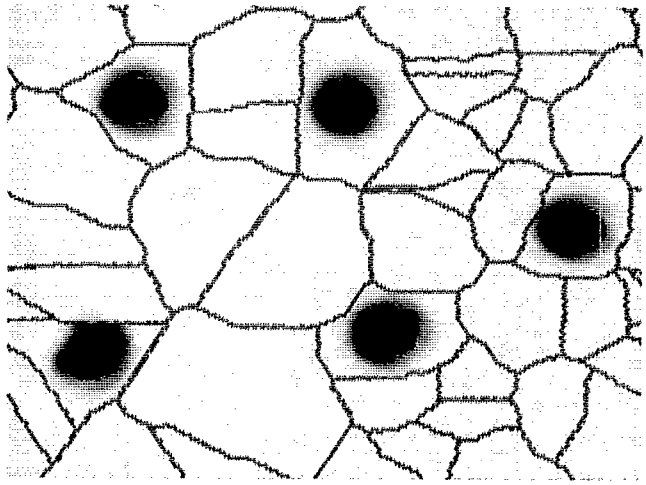

(a)

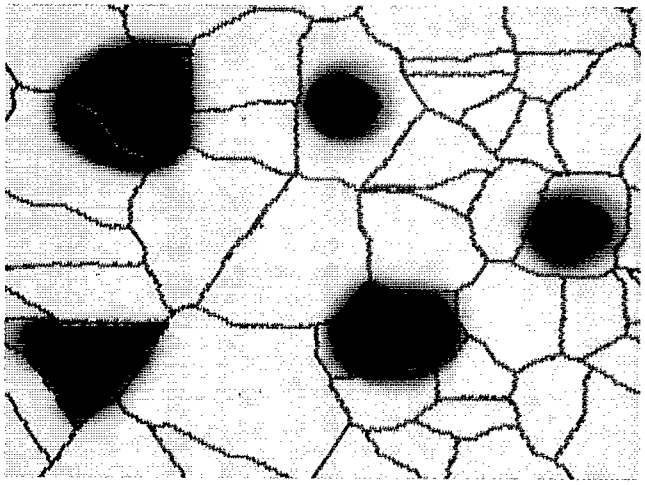

(d)

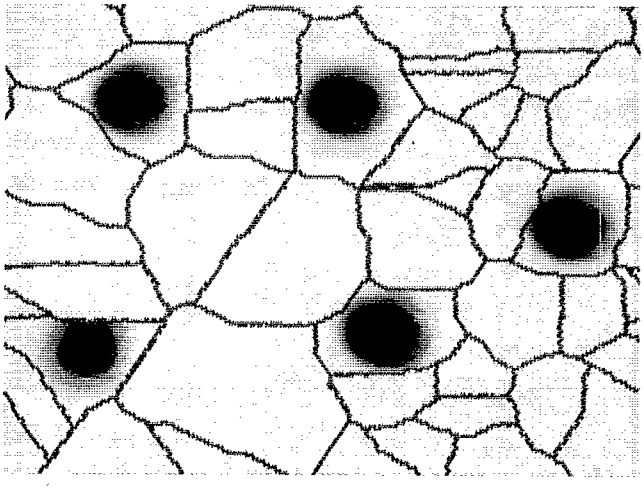

(b)

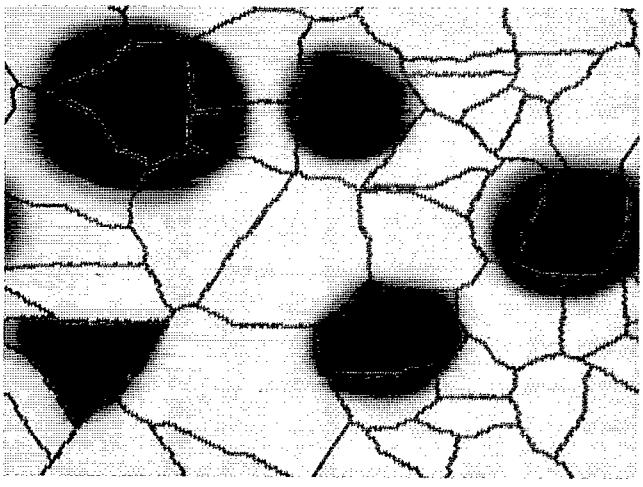

(e)

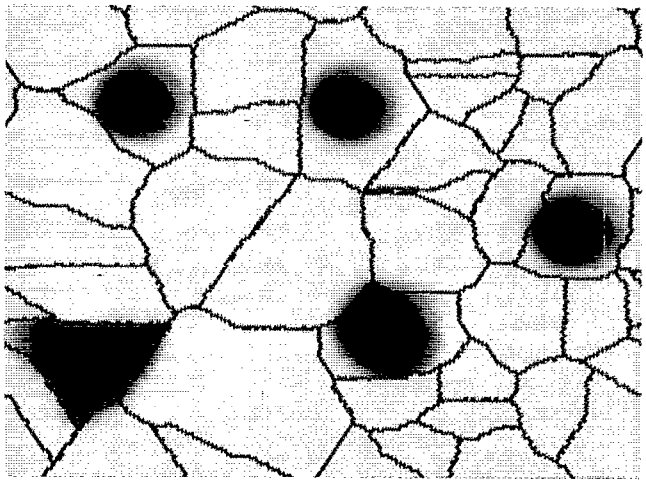

(c)

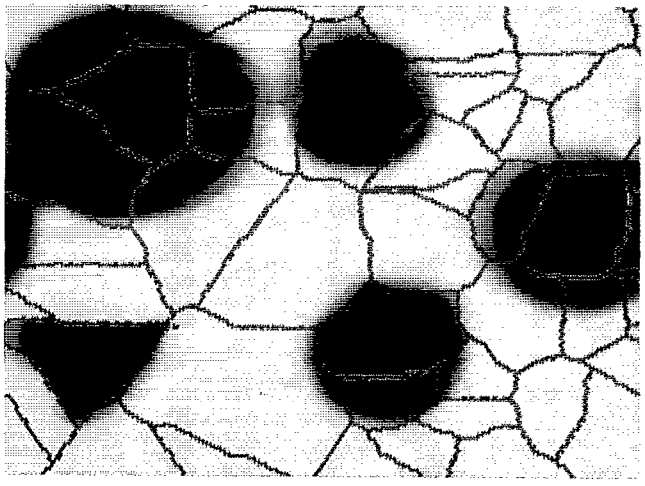

(f)

FIG. 2. Effects of patch borders on domain wall motion for the patchy film described in Sec. I. (a) The initial state has five reverse domains. These domains are located inside patches whose borders have 10% (lower left), 20% lower right, 30% (upper left), 40% (upper right), and 50% (middle right) exchange strength. (b) The remnant state. (c) The steady state under $H_z = -1$ kOe. (d) The steady state under $H_z = -1.5$ kOe. (e) and (f) Evolution starting from (d) under $H_z = -2$ kOe at 0.95 and 1.25 ns.

tween the easy axis and the $+Z$ direction, and ϕ_a is the azimuthal angle of the easy axis in X-Y plane. To fix $\mathbf{e}_a$ for each site, we let θ_a have an equal probability to be any value within (0,45°), and *independently*, let ϕ_a have an equal probability to be any value within (0,360°). Later we will refer to such an orientational distribution simply by saying that the easy axes are randomly oriented in a 45° cone about the perpendicular direction. In Appendix A we will show that the average anisotropy of such a distribution is uniaxial with the easy axis perpendicular to the film plane and with the average anisotropy constant $\langle K_1 \rangle = 0.727 K_1$. Since the domain wall width ($\simeq 100$ Å) covers many sites, the site to site randomness does not affect the dynamics, except that it reduces the average anisotropy constant.

The stiffness constant is set to different values at the patch borders. To study domain wall motion and domain expansion, we have prepared five reverse domains as the initial condition; see Fig. 2(a). To keep these initial nuclei from shrinking, K_1 at the central disk of each reverse domain is set to be 10^7 erg cm^{-3}, which is ten times the nominal value. For the five patches containing a reverse domain, starting from the lower left corner and moving counterclockwise, A_x on the patch borders are set to be 10%, 20%, 50%, 40%, and 30% of the nominal value of 10^{-7} erg cm^{-1}. On all the remaining borders A_x is equal to 50% of the nominal value.

Figure 2(a) shows the initial magnetization state. Five reversed domains are artificially created in the film. Following the direction change in each of the domain wall, we see that the accumulated winding angle is equal to 2π for each domain wall. Now we let this initial magnetic state relax to the remnant state shown in Fig. 2(b). During the process the lower left domain with 10% exchange on the patch borders changes dramatically, while the remaining four domains with higher exchange (20% or more) on the borders remain almost the same. One change of the lower left domain is that the domain expands to the north border of the patch. The reason is that the domain wall is initially close to the border which has only 10% exchange energy. Therefore, it sticks to the border to minimize the wall energy, just as a domain wall sticks to a void region as shown in Refs. [10] and [11]. In other words, we can say that a patch border with weak exchange has a tendency to attract the domain wall. Another change is that the winding number becomes zero; i.e., the dipoles in the domain wall region align in the same direction. This change is also due to the weaker exchange on the patch borders. If there were no such borders, the winding number would not have been changed, since changing a winding number must create antiparallel dipoles which corresponds to a higher exchange energy. In the present case of weak exchange coupling there is no such exchange energy barrier.

Now we investigate the coercivity of domain wall motion by applying a magnetic field H_z in the $-Z$ direction. At first, we apply $H_z = -1$ kOe to the remnant state and obtain the steady state shown in Fig. 2(c). Now the lower left domain expands to fill the whole patch, since both the external field and the patch border of small A_x help the domain expand. However, when the domain reaches the border, the weak exchange interaction prevents it from crossing over. Thus the domain is confined within the patch. At the next stage, we increase the field to $H_z = -1.5$ kOe. The new steady state is displayed in Fig. 2(d). Since the domain in the lower left corner is more or less disconnected from other patches, it does not have much influence outside the patch. Therefore, for the domain wall to move beyond the patch, the external field must overcome the nucleation coercivity, which is about $2\langle K_1 \rangle / M_s - 4\pi M_s = 13$ kOe and is much higher than the present field strength of 1.5 kOe. This picture also applies to the patch whose borders have 20% exchange; see the reversed domain in the lower right corner in Fig 2(d). In contrast to the cases of weak exchange, the domain in the extreme right with borders of 50% exchange and that in the upper central patch with borders of 40% exchange do not expand much. The reason why the domain within a patch of weaker exchange borders is easier to expand (within the patch) is that, the dipoles outside the domain but inside the patch are primarily influenced by the domain, which tends to reverse them. If the exchange on the patch borders are strong, then the dipoles are not only influenced by the domain, but also by the region outside the patch, which tends to hold them upward. In other words, when the domain is near the patch border, the upward dipoles outside the patches exert an exchange force on the dipoles inside the patch to prevent the reversal. Consequently, within a patch, the smaller the exchange on the patch borders, the lower the wall motion coercivity.

The reverse domain in the upper left corner with 30% exchange at the patch borders shows a compromise case, as illustrated in Fig. 2(d). Here, the coercivity of domain wall motion is below 1.5 kOe. When the domain touches the borders, the exchange force of the reversed domain and the external field together make the domain expand slightly into the neighboring patches. It then stops inside the patches, pinned by the low exchange patch border. Now we increase the field to $H_z = -2$ kOe. Figure 2(e) and (f) are snapshots of the magnetization states after the system evolves for 0.95 and 1.25 ns from the state shown in Fig. 2(d). Now H_z is strong enough to force the wall move outward and the four domains with relatively stronger exchange interaction at the borders expand, until eventually the whole film is reversed (the final state is not shown). In the process the domain in the lower left corner does not expand, because the applied field is still much weaker than the nucleation field ($\simeq -13$ kOe), as was mentioned before.

The above simulations show that, in the vicinity of patch borders (within distance of the domain wall width), the wall motion is much affected by the exchange strength on the patch borders. The lower exchange borders (e.g., 10% and 20% in the present film) make the domain easy to expand within the patch, but prevent the domain wall from crossing the patch border. The opposite is true for patches with higher exchange strengths (e.g., 40% and 50%). The domain in a patch with borders of intermediate exchange strength (e.g., 30%) can expand most easily to the whole film, because the exchange strength on the borders is low enough to let the domain grow within the patch and high enough to let the domain cross the patch borders.

II. DEMAGNETIZATION IN A PATCHY FILM

Now we consider a patchy film which has a relatively high saturation magnetization, but has zero exchange on all the

patch borders. The main feature of such a patchy film is that it can be easily demagnetized under an external field leading to irreversible $M-H$ curves. The purpose of these simulations is to understand the mechanism that leads to demagnetization and irreversible processes observed in several magneto-optical thin films, e.g., the Co/Pt superlattices.[12] The physics of the demagnetization process will be explained later, following the presentations of the simulation results.

The film is specified as follows. The film thickness $h = 1000$ Å, saturation magnetization $M_s = 410$ emu cm^{-3}, anisotropy constant $K_1 = 2\times 10^6$ erg cm^{-3}. The easy axes are randomly distributed from site to site on the original hexagon lattice, within a 45° cone about the $+Z$ direction, in the manner explained in Sec. I. The average anisotropy constant is $\langle K_1\rangle = 0.727K_1 = 1.5\times 10^6$ erg cm^{-3}, where the factor 0.727 is derived in Appendix A.

The film contains 481 complete patches with random shapes and sizes as shown in Fig. 3. The exchange stiffness coefficient $A_x = 10^{-7}$ erg cm^{-1} within the patches and is set to be zero at all the patch borders. The average dimension of the patches is about 100 Å. This dimension is comparable to the domain wall width $\pi\sqrt{A_x/\langle K_1\rangle} \simeq 80$ Å.

Now we explain why the patchy film can be easily demagnetized. When all the patches are magnetized in the $+Z$ direction, each patch will experience a magnetic field in the $-Z$ direction produced by all the other patches due to the magnetic dipole–dipole interaction. A dipole also experiences the demagnetizing field produced by other dipoles in the same patch. However, this is an internal field and does not affect the magnetic behavior of the patch, provided that the patch is small (so that the shape effect in the patch is negligible) and the dipoles move as a whole due to the strong exchange coupling. In Appendix B we will present analytical results for a circular patch (i.e., the volume covered by the patch is a cylinder) in a perpendicularly magnetized film. The demagnetizing field on the circular patch is approximately

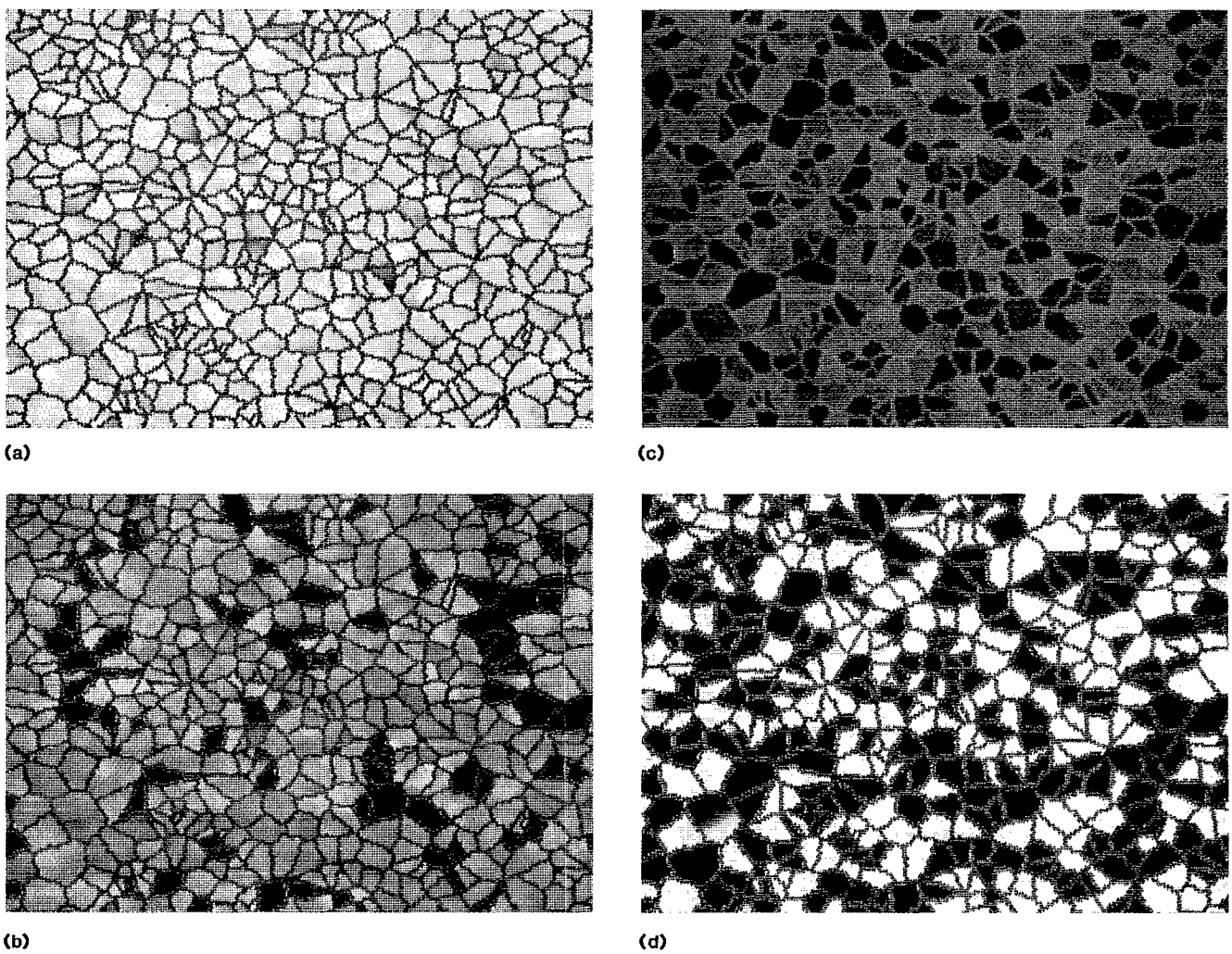

FIG. 3. Demagnetization under an in-plane applied field for the patchy film described in Sec. II. (a) The steady state under $H_x = 500$ Oe. Two small patches are reversed due to the applied field and the demagnetizing field. (b) The steady state under $H_x = 2$ kOe has more reversed patches. (c) As the field is increased to $H_x = 6$ kOe, almost half of patches are reversed. (d) The fully demagnetized state with zero magnetization is reached when the film is firstly saturated in the $+X$ direction under $H_x = 8.5$ kOe and then evolves under zero field.

$$H_{\text{demag}} = -4\pi M_s [h/(r+\sqrt{r^2+h^2})] , \qquad (2)$$

where r is the radius of the cylinder. In calculating H_{demag} we have assumed that the dipoles outside the circular patch are all in the $+Z$ direction. If some regions are already reversed, the demagnetizing field will become weaker. This equation tells us that the demagnetizing field on a patch is stronger if the patch is smaller, the film is thicker, and saturation magnetization is larger. Using $r = 50$ Å, $h = 1000$ Å, and $M_s = 410$ emu cm^{-3}, we find for an *average* patch $H_{\text{demag}} \simeq 5$ kOe, while the anisotropy field $H_{\text{ani}} = 2\langle K_1 \rangle / M_s \simeq 7.1$ kOe.

We performed two series of simulations to obtain the in-plane and perpendicular $M-H$ curves. Figure 3 illustrates the magnetic states under in-plane external fields along the $+X$ direction. The dipoles are initially set in the $+Z$ direction. Then we let them evolve under zero external field to the remnant state. The remnant state has a magnetization of 99.2 emu cm^{-3} in the $+Z$ direction. Figure 3(a) shows the steady state under $H_z = 500$ Oe. The light red color shows that the magnetization has, to some extent, tilted from $+Z$ to $+X$ direction. Here, two small patches are already reversed. The in-plane applied field helps the magnetization move away from the easy axis (the $+Z$ direction) and makes reversal easier. However, an in-plane field alone will not cause reversal. The reversal is due to the demagnetizing field produced by other patches and it is made easier by the zero exchange on the patch borders. Figure 3(b) shows the steady state under $H_x = 1$ kOe. The patches with dark colors have been reversed and those with light colors are between the $+X$ and $+Z$ directions. The red in the background of both the light and dark patches shows that all the patches have a $+X$ magnetization component. Figure 3(c) shows the steady state under $H_x = 6$ kOe, where about half of the patches are reversed. When the externally applied in-plane field is removed, the film will become fully demagnetized with zero magnetization; see Fig. 3(d). The $M-H$ curves becomes irreversible once the first reversal occurs.

In the simulations, we increased H_x stepwise from 0 to 8.5 kOe with a step of 250 Oe. For each increase we let the film evolve from the previous steady state to reach the new steady state. Throughout this paper we let $\mathbf{M} = (M_x, M_y, M_z)$ be the magnetization vector *averaged* over the whole film and $M = |\mathbf{M}|$ (remember that M_s is the amplitude of the local magnetization). Obviously, we have generally $M \leqslant M_s$, where the equality holds if and only if all the dipoles are oriented in the same direction. The difference $(M_s - M)$ describes the extent of incoherence of the dipole moment orientations. Since no field is applied in the Y direction, $M_y \simeq 0$ always holds. We are thus interested in M_x, M_z, and M as functions of external field. The $M-H$ curves for the simulations described above are plotted in Fig. 4. It is interesting to notice that the $M_x - H_x$ curve here resembles that observed in the Co/Pt superlattice films.[12] That is, M_x increases first with a steep slope. Then, as more and more patches are reversed, the slope becomes flatter, until $\mathbf{M}$ is saturated in the $+X$ direction. This slope change is due to the demagnetizing field and the reversed patches. At first glance, one may think that a reversed patch should contribute the same amount of increase to M_x as the unreversed patches. If this were true, the $M_x - H_x$ slope would not have changed at the field where the patches begin to reverse. It turns out that there is a major difference between a reversed and an unreversed patch, as long as only a few isolated patches are reversed. That is, the demagnetizing field which is produced mainly by the unreversed patches and is thus in the $-Z$ direction, reduces the effective anisotropy field for unreversed patches, but enhances it for reversed patches. Therefore, the reversed patches are more tightly bound in the $-Z$ direction and make less contribution to M_x. This is why the slope of the $M_x - H_x$ curve becomes smaller when more patches are reversed.

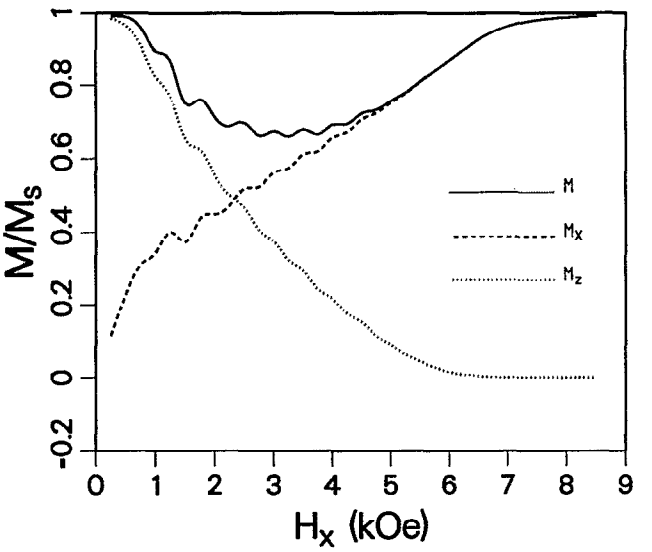

FIG. 4. M, M_x, and M_z as functions of H_x for the patchy film described in Sec. II. The $M_x - H_x$ curve is steep for weak H_x and flatter for strong H_x, resembling the observed behaviors in the Co/Pt superlattice.[12]

Next we applied a field in the $-Z$ direction ($H_z < 0$). The magnetization states are shown in Fig. 5. Again, H_z is changed stepwise from zero to -13.5 kOe in steps of 250 Oe. The film is initially saturated in the $+Z$ direction. The demagnetizing field at first helps the patches to reverse. Then, as more patches are reversed, the demagnetizing field changes to the $+Z$ direction and becomes opposite to the external field. Therefore, for the first patch to reverse we need $|H_z| \simeq H_{\text{ani}} - |H_{\text{demag}}|$, while for the last patch to reverse we need $|H_z| \simeq H_{\text{ani}} + |H_{\text{demag}}|$. That is why the first two small patches are reversed at only $H_z = 750$ Oe [Fig. 5(a)], and about one half of the patches are reversed at $H_z = -7$ kOe [Fig. 5(b)], and even at $H_z = -13.5$ kOe there are still two patches remaining upward [Fig. 5(c)]. The $M_z - H_z$ curve is shown in Fig. 6. Since there is no exchange on the patch borders, the reversed domain cannot expand and the corresponding hysteresis loop is sheared.

In summary, a patchy film will show the following effects if the saturation magnetization is large, the patches are small (compared to the film thickness), and the exchange on the patch borders is weak. When an in-plane external field is applied to such a film, the reversed and

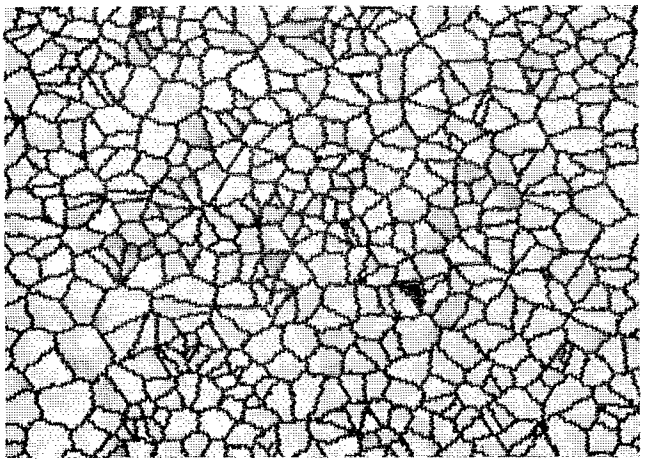

(a)

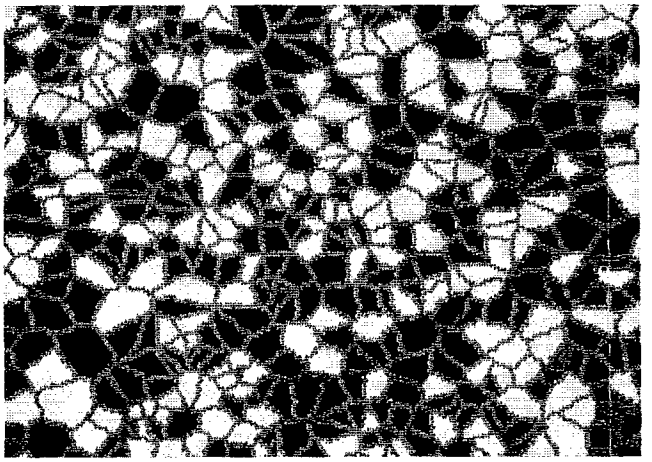

(b)

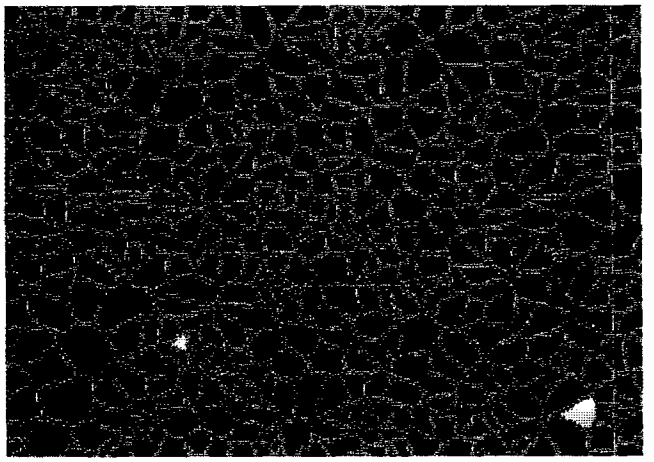

(c)

FIG. 5. Demagnetization under perpendicularly applied fields H_z for the patchy film described in Sec. II. (a) Two small patches are reversed for $H_z = -750$ Oe. The demagnetizing field helps reverse when only a few patches are reversed. (b) About half of the patches are reversed for $H_z = -7$ kOe. (c) Under $H_z = -13.5$ kOe there are still two unreversed patches, since the demagnetizing field is against the reverse.

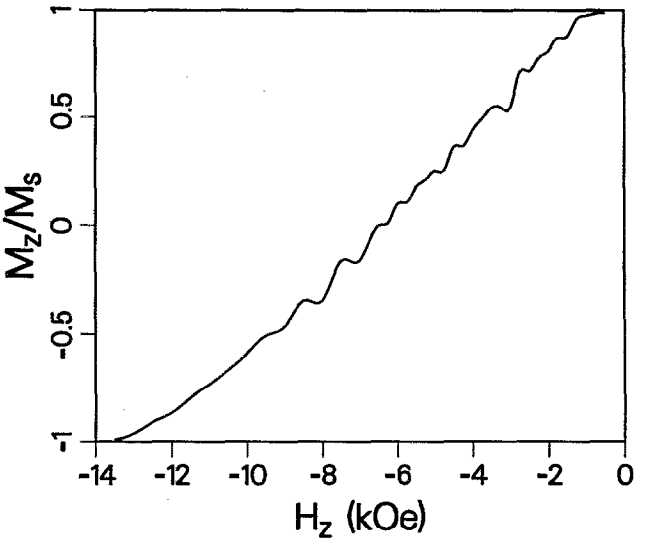

FIG. 6. M_z as a function of H_z for the patchy film described in Sec. II. This curve has a poor squareness because there is no exchange coupling on the patch borders.

unreversed patches will respond differently, causing the $M_x - H_x$ curve to be steep at weak H_x and flatter at strong H_x. When a perpendicular field is applied opposite to the magnetization ($-Z$ direction), the demagnetizing field helps the external field to make the first few patches reverse, but will make it harder to fully saturate the film in the $-Z$ direction.

The demagnetizing effects may play a role in the $M_x - H_x$ and $M_z - H_x$ behaviors of a multilayered Co/Pt film studied by Hajjar, Mansuripur, and Shieh in magnetoresistance measurements.[12] The Co/Pt film has a saturation magnetization $M_s = 410$ emu cm^{-3} and is believed to have polycrystalline structures. The observed $M_x - H_x$ has a steep slope for weak H_x and it becomes flatter with increasing H_x. The observed $M_z - H_x$ curve has a shoulder at $H_x \simeq 3$ kOe. Below this field the curve is repeatable and has a shape which can be described by the Stoner–Wohlfarth theory. Above that shoulder point, the curve is not repeatable. These features agree qualitatively with the simulation curves shown in Fig. 4. In contrast to Fig. 6, the observed $M_z - H_z$ curve has a good squareness. This difference between the experiment and the simulation results from the assumption that there is no exchange on the patch borders. Comparing Secs. III and IV with Appendix C, we will see that a weak exchange (e.g., 20%) on the patch borders is enough to produce a perpendicular hysteresis loop with sharp squareness, but it will not cause much change in the in-plane $M - H$ curves. When we allow the simulated patch borders to have a weak but nonzero exchange, both the in-plane and perpendicular magnetic behaviors agree qualitatively with the observed curves.

III. PATCHY FILM WITH RANDOM EASY AXES

In Secs. I and II the easy axes are oriented randomly from site to site on the original hexagonal lattice. However, since

the exchange energy for each dipole is much stronger than the anisotropy energy, the dipoles are tightly coupled in one direction and do not feel the individual easy axes. Specifically, the exchange energy of a dipole interacting with its six nearest neighbors in the hexagonal lattice is equal to $2\sqrt{3}A_x h$, and the anisotropy energy is equal to $\sqrt{3}a^2 hK_1/2$. For $a = 10$ Å, $A_x = 10^{-7}$ erg cm^{-1} and $K_1 = 10^6$ erg cm^{-3}, the exchange energy is about 40 times the anisotropy energy. In this case, the dipoles only feel the average easy axis of the patch, which is perpendicular to the film plane. The site-by-site randomness is averaged out, causing only a reduction of the average anisotropy constant.

In this section we investigate a patchy film in which the easy axes are along the same direction in each patch but are different from patch to patch. In the next paragraph we will show that for this film the exchange coupling at borders of a patch is comparable to the anisotropy energy of the whole patch and it cannot bring the dipoles in different patches to align. Therefore, the random orientations of the easy axes will not be averaged out. We want to study how such a random anisotropy may affect the magnetic properties.

The patchy film is specified as follows. The film thickness $h = 500$ Å, the saturation magnetization $M_s = 100$ emu cm^{-3}, and the anisotropy constant $K_1 = 10^6$ erg cm^{-3}. The anisotropy axes are oriented in the same direction within each patch, but they are randomly oriented in different patches in a 45° cone about the film's normal direction. The film contains 441 complete patches with random shapes and sizes. The exchange stiffness coefficient $A_x = 10^{-7}$ erg cm^{-1} within a patch and $A_x = 0.2\times 10^{-7}$ erg cm^{-1} on the patch borders. The average dimension of the patches is about 110 Å, which is comparable to the domain wall width $\pi\sqrt{A_x/K_1} \simeq 100$ Å. Now we estimate the ratio of the exchange energy at the patch borders to the anisotropy energy for an average patch. Assume that the patch is square in shape and its side has a length of $L_p = 110$ Å. Then the exchange energy around the patch border if $4L_p A_x h/a$ (where A_x is for the borders), while the anisotropy energy of the patch is about $L_p^2 hK_1$. Using the values given above, the ratio of the exchange energy to the anisotropy energy is close to one (0.73). This amount of exchange energy cannot make the dipoles on different patches to be parallel. The patches will thus move more or less independently under given external field, leading to incoherent and irreversible processes. In the following we present the simulation results. Results based on a statistical Stoner–Wohlfarth theory will be presented in Appendix C, where we first apply the Stoner–Wohlfarth theory[13,14] to each individual patch and then find the average magnetization for all the patches.

To obtain various $M - H$ curves, we applied, respectively, an in-plane field, a perpendicular field, and a rotating field to the film. In the former two cases the applied field strength is increased from zero at a rate of 100 Oe ns^{-1}. In the third case we keep the amplitude of the field to be constant and rotate the field vector at a rate of 10° ns^{-1}. Except in the vicinity of the critical point, the rates are slow enough to allow the magnetization state at any time to be actually the steady state under the corresponding *constant* field.

Figure 7 shows the magnetization states under the in-plane applied fields H_x. The film is initially saturated in the $+Z$ direction. Then we let it evolve under zero field to the remnant state as shown in Fig. 7(a). Different colors indicate the magnetization vectors are along different directions, because the patches have different easy axes. The average magnetization of the remnant state is equal to $M_{\text{rem}} = 94.5$ emu cm^{-3}, which is smaller than the nominal value of the saturation magnetization $M_s = 100$ emu cm^{-3}. The blue patches are of particular interest, because their easy axes are near the vector $(x,y,z) = (-1,0,1)$, which has a 135° angle with the applied field. According to the Stoner–Wohlfarth theory,[10,14] the magnetization vectors of these patches will jump discontinously towards the vector $(x,y,z) = (1,0,-1)$ at $H_x = 0.5H_k$, where H_k stands for the effective anisotropy field. Since the magnetization vector will not return to its original state as the field is decreased, the jump is irreversible. Using $H_k \simeq 2K_1/M_s - 4\pi M_s = 19$ kOe (the approximation comes from the fact that the local easy axis is not perpendicular to the film plane), the jump should occur at about $H_x = 9.5$ kOe, if there is no exchange between the patches. For patches having easy axes in other orientations the jump requires a higher H_x. In the patchy film this field can be reduced or increased, depending on the easy axes of the neighboring patches. Figure 7(b) shows the magnetization state under $H_x = 5.9$ kOe. Up to this filed strength, all the magnetization vectors move continuously toward the $+X$ direction. Figure 7(c) shows the magnetization state when H_x is increased to 7.4 kOe. Now several patches become dark red, indicating that the magnetization vectors of the patches have experienced the jump. These patches were blue in the initial state. The jumps result in an abrupt increase in M_x and a decrease in M_z. At this point the rotation of the magnetization becomes irreversible; i.e., it will not return to the initial state when H_x is reduced to zero. As H_x is further increased, more jumps occur. Figure 7(d) shows the state under $H_x = 8.7$ kOe. Due to the exchange coupling, a jumped patch will induce jumps in the neighboring patches, thus leading to nucleations around the initially blue patches.

We continuously increased H_x from 0 to 12.5 kOe. Figure 8(a) shows M, M_x, and M_z as functions of H_x. Here we see that M_x first increases linearly with increasing H_x. In the linear regime all the magnetization vectors move continuously toward the applied field. Figure 8(b) shows the magnified M and M_z curves of Fig. 8(a). Here we see that, since the dipoles are better aligned when the field is increased, the amplitude of the average magnetization increases with the increasing applied field. Neglecting this increase will cause an error in the measurement of $\langle K_1 \rangle$. We will come back to this point later. Then the $M_x - H_x$ curve shows steeper slope, corresponding to the jumps of some patches. The jumps lead to an increase in M_x, but a decrease in M_z. Now the demagnetization begins and the process becomes irreversible. The drop in M indicates that the movements of the magnetization vectors are highly incoherent. They align again in the $+X$ direction when H_x is sufficiently high. It is interesting to notice the small cascades in the $M_z - H_z$ curve. These cascade plateaus occur when the reversed and unreversed magnetization vectors

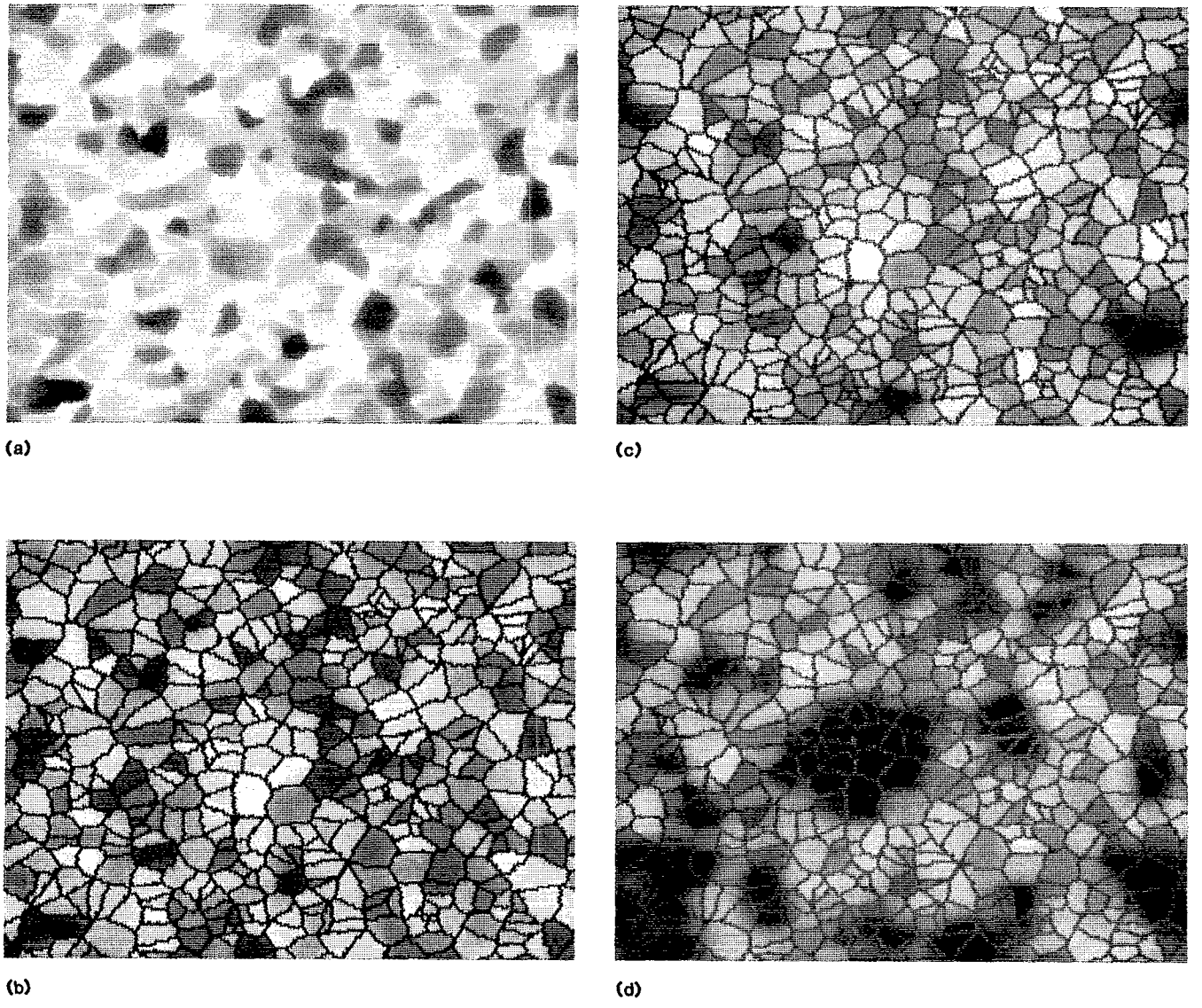

FIG. 7. Magnetization state under in-plane applied field H_x for the patchy film described in Sec. III. (a) The remnant state. (b) The state at $H_x = 5.9$ kOe. Up to now the magnetization vectors have moved continuously with increasing H_x. (c) As H_x is increased to 7.4 kOe, some of the initially blue patches become dark red, indicating that the discontinuous jump described in the Stoner–Wohlfarth theory occurs. (d) As H_x is increased to 8.7 kOe, all the initially blue patches have passed the jump point and become dark red.

rotate toward the in-plane applied field. One increases M_z and the other decreases M_z, leading to the plateaus of the cascades.

Since it behaves smoothly in the low field regime, the observed M_z vs H_x has been suggested to be used to measure the anisotropy constant.[15] In this approach the magnetization in the remnant state M_{rem} is treated as saturation magnetization and the angle between the magnetization and Z axis is calculated by the relation $M_z = M_{\text{rem}} \cos \theta_m$. The best fit between the experimental data and the Stoner–Wohlfarth theory (which ignores the nonuniformity of the film) gives anisotropy constant $\langle K_1 \rangle$. However, the measurements of the multilayered Co/Pt and Co/Pd samples showed that $\langle K_1 \rangle$ measured in this way is usually several percent larger than that measured by using a rotating field.[16] Now we take the simulated $M_z(H_x)$ curve as given data, and use the Stoner–Wohlfarth theory[10] to match it. The best fit between the simulation curve and the theory for $M_{\text{rem}} = 94.53$ emu cm^{-3} in the range of $0 \leqslant \theta_m \leqslant 15°$, which corresponds to $0 \leqslant H_x \leqslant 5$ kOe, yields $\langle K_1 \rangle = 1.0 \times 10^6$ erg cm^{-3}. Later we will compare this value with the simulations that uses a rotating field, and explain why $\langle K_1 \rangle$ found by using an ion-plane field is higher than its actual value.

Now we discuss the case of applying a perpendicular

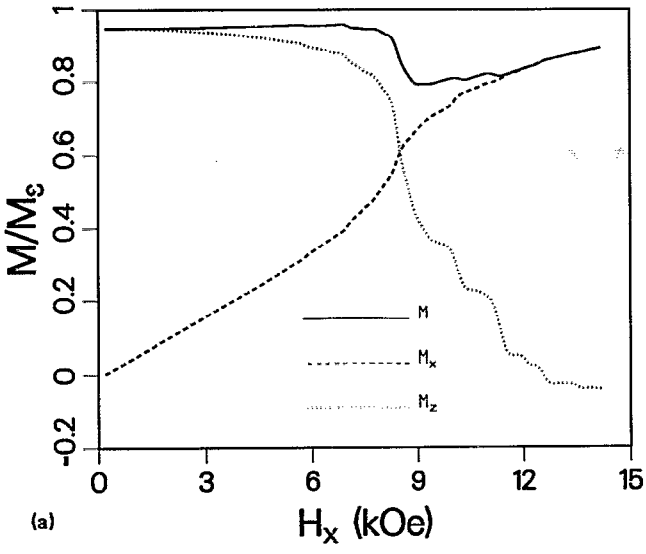

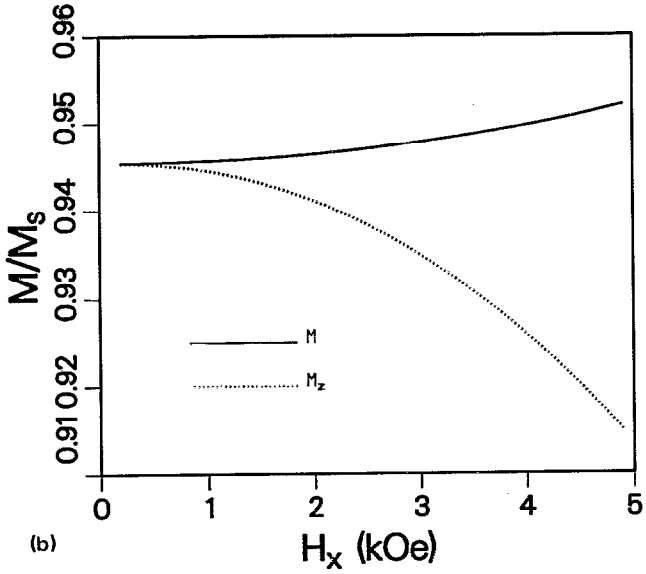

FIG. 8. (a) In-plane $M - H$ curves for the patchy film described in Sec. III. The point at which M_x increases and M_z decreases at a steeper slope marks the occurrence of the discontinuous jumps in some patches. The M_z curve shows cascades. $\langle K_1 \rangle$ found by the best fit of the $M_z - H_x$ curve is equal to 1.0×10^6 erg cm^{-3}. (b) Enlarged M and M_z curves shown in (a) for $0 < H_x < 5$ kOe, showing M increases with increasing H_x.

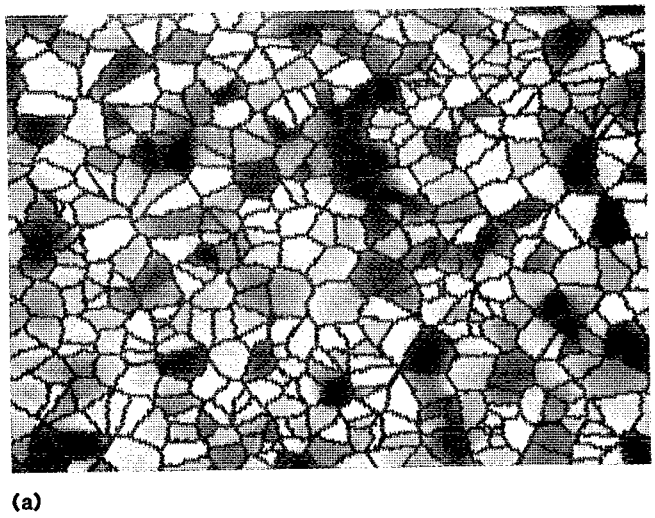

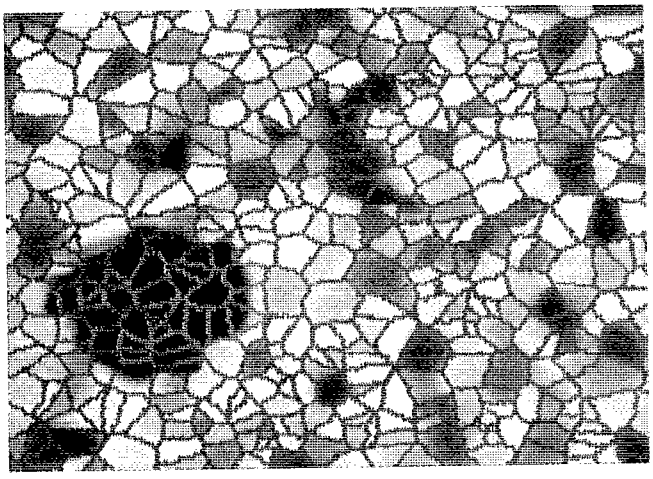

FIG. 9. Magnetization state under perpendicular applied field H_z for the patchy film described in Sec. III. H_z is changed from zero at a rate of -100 Oe ns^{-1}. (a) The magnetization vectors move continuously to the film plane as H_z is changed to -10335 Oe. (b) As H_z is increased to -10360 Oe, a domain is reversed. It will expand quickly to the whole film, so that the hysteresis loop has a very sharp squareness.

field H_z. We start from the remnant state shown in Fig. 7(a). Since some easy axes are 45° away from Z axis, the minimum field for the discontinuous jump to occur is again about 10 kOe. Figure 9(a) shows the state at $H_z = -10\,335$ Oe. The magnetization state has $M_z = 0.83M_s$ and is still close to the remnant state (where $M_z = 0.95M_s$). As the field is increased slightly further to $H_z = -10\,360$ Oe, a reversed domain centered at an initially blue patch occurs, see Fig. 9(b). The domain soon expands to the whole film, so the hysteresis loop has a very high squareness; see Fig. 10. This is expected because the wall motion coercivity is usually much lower than the nucleation coercivity (e.g., in the film discussed in Sec. I the wall motion coercivity is less than 2 kOe), unless severe barriers exist to wall motion.

Another common situation in magneto-optical measurement is that an external field with constant amplitude H_{ext} is rotated about the film. Recent measurements on the multilayered Cd/Pt and Co/Pd films showed that in this case the measured anisotropy constant $\langle K_1 \rangle$ is generally smaller (by up to 10%) than that measured by applying an in-plane field. Now we simulate this situation. We start from the remnant state shown in Fig. 7(a). In the first run we let $H_{ext} = 7$ kOe and let the field rotate from the $+Z$ to $-Z$ direction in the X-Z plane. Figure 11(a) shows the magnetization state for $\alpha = 98°$, where α is the angle between the field and the Z axis ($\alpha = 90°$ means that the field is along X). Here we see that several initially blue patches

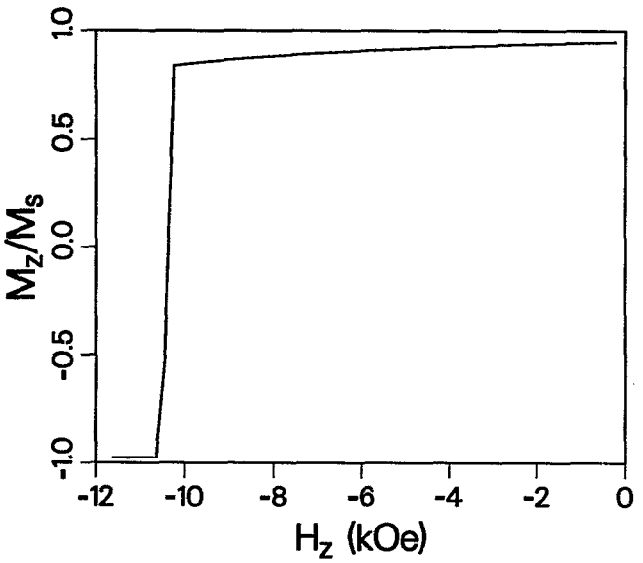

FIG. 10. Perpendicular hysteresis loop for the patchy film described in Sec. III. The loop shows a sharp squareness even if the exchange on the patch borders is 20% of the nominal value.

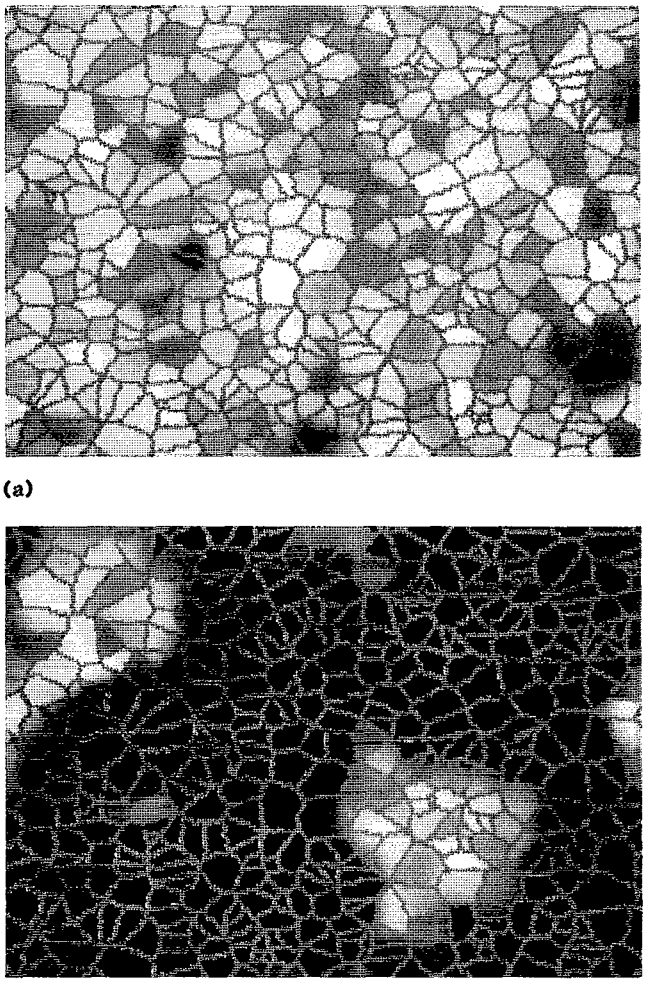

FIG. 11. Magnetization states for rotating field with $H_{ext} = 7$ kOe for the patchy film described in Sec. III. (a) $\alpha = 98°$, where α is the angle between the field and Z axis. The initially blue patches as shown in Fig. 7(a) first become dark red. (b) $\alpha = 118°$. The reversed patches serve as nucleation centers. The initially red patches are most difficult to reverse.

[see Fig. 7(a)] become dark red, indicating that they have a negative M_z component. These patches have experienced the discontinuous jump as described by the Stoner–Wohlfarth theory. Figure 11(b) shows the state for $\alpha = 118°$, where more patches are reversed around the dark red patches shown in Fig. 10(a). Few changes take place in the initially red patches, where the easy axes are near to or along the vector $(x,y,z) = (1,0,1)$. This is expected from the Stoner–Wohlfarth theory, because the angle between the easy axes and the field are not large enough to cause the jump. As the field is further rotated toward the $-Z$ direction all patches reverse, because the Z component of the field exceeds the wall motion coercivity.

We also did the simulations for $H_{ext} = 10$, 15, and 20 kOe. M, M_x, and M_z as functions of the field angle α for different H_{ext} are plotted in Fig. 12. The different depths of the dip in the function $M(\alpha)$ show that the magnetization vectors of the patches move more coherently for $H_{ext} = 15$ and 20 kOe, but less uniformly for $H_{ext} = 7$ and 10 kOe. The reason is that the randomness of the easy axes, which tends to cause the incoherence, is suppressed in the cases of strong external fields. Now we use the Stoner–Wohlfarth theory to match the four $M_z(\alpha)$ curves. Since there are random easy axes, the magnetization M is not a constant, but a function of the field amplitude and direction. As in the experiment we use $M(H_{ext}, \alpha = 0)$ as the saturation magnetization, which is the average magnetization when the applied field is along the $+Z$ direction, and use $M_z = M(H_{ext}, \alpha = 0)\cos\theta_m$ to calculate θ_m. Obviously, due to the alignment of the dipole moments along the field, $M(H_{ext}, \alpha = 0)$ is larger than M_{rem}. But the magnetization then does not change as the field rotates; see Fig. 12(e). Therefore, the motion of the magnetization is more coherent and can be better described by the Stoner–Wohlfarth theory than in the case of applying an increasing in-plane field. For the four cases in Fig. 12 we have M (7 kOe, 0°) = 96.75, M(10 kOe, 0°) = 97.32, M(15 kOe, 0°) = 98.00, and M(20 kOe, 0°) = 98.46 emu cm^{-3}, which are about 2% to 4% larger than $M_{rem} = 94.53$ emu cm^{-3}. For $0 \leqslant \theta_m \leqslant 15°$, the four $M_z(\alpha)$ curves in Fig. 12 (a)–(d) are best fitted by $\langle K_1 \rangle = 0.89$, 0.91, 0.92, 0.91×10^6 erg cm^{-3}, respectively. These values differ slightly from each other, but they are about 10% smaller than the value $\langle K_1 \rangle = 1.0 \times 10^6$ erg cm^{-3} found from the simulation curve under the in-plane applied field. This is the same difference as observed in the measurements. Since the motion of the dipoles is more coherent under rotating field, K_1 measured in this case is more accurate. In contrast to the case of rotating field, the average magnetization amplitude M in the case of in-plane applied field increases with the increasing field; see Fig. 8(b). If one neglects this in-

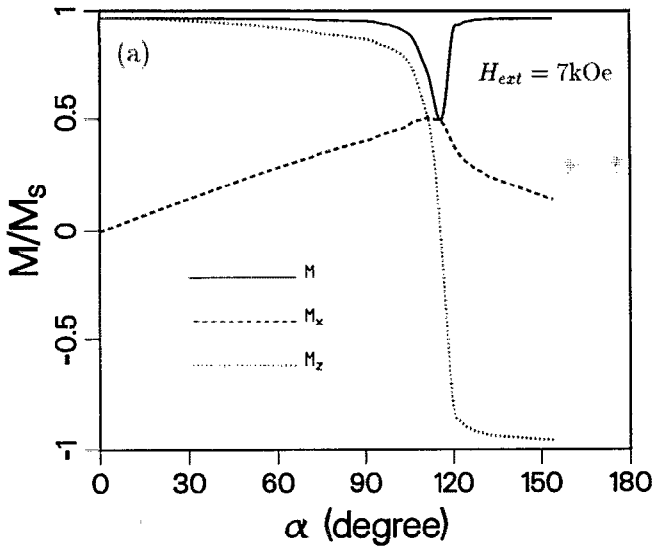

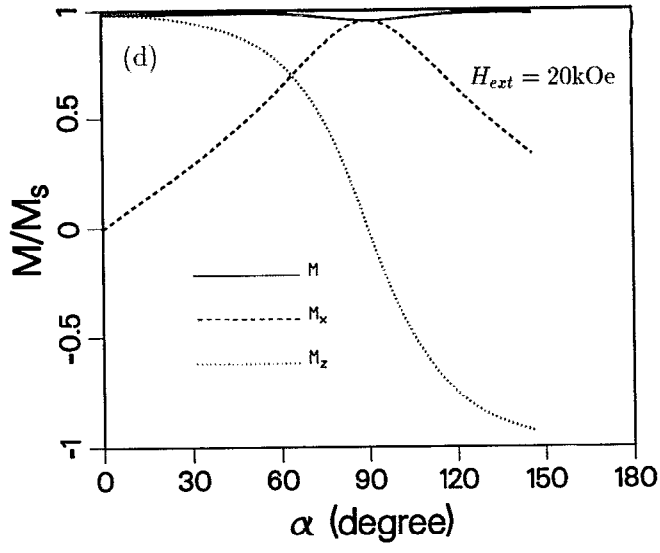

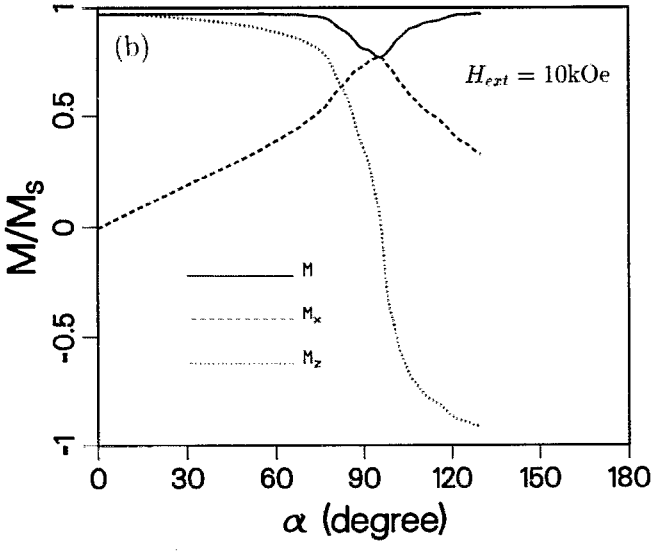

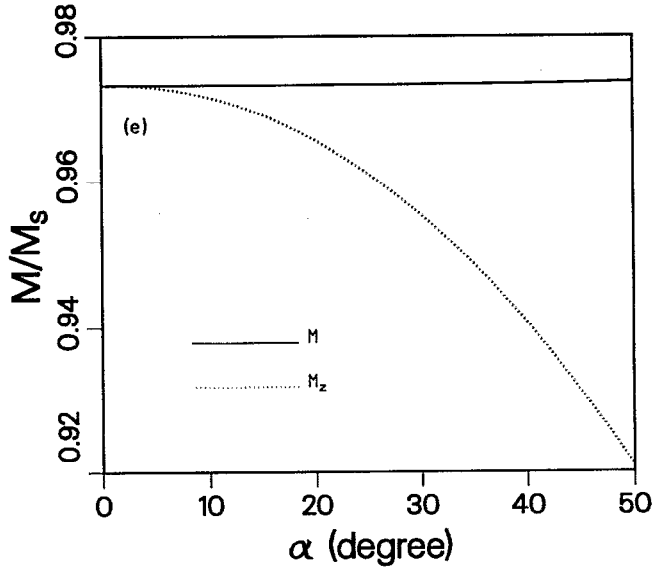

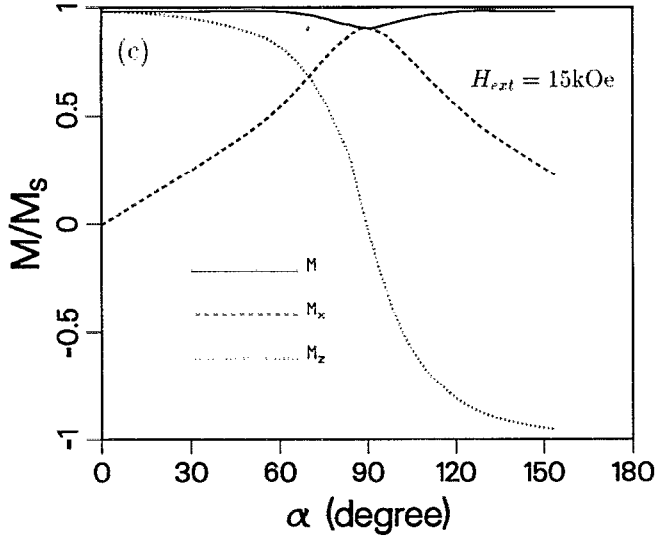

FIG. 12. M, M_x, and M_z as a function of the field angle α for different amplitude H_{ext} for the patchy film described in Sec. III. (a) H_{ext} = 7 kOe. (b) H_{ext} = 10 kOe. (c) H_{ext} = 15 kOe. (d) H_{ext} = 20 kOe. (e) Enlarged version of (b) for $0 \leqslant \alpha \leqslant 50$, showing M is a constant as α changes. $\langle K_1 \rangle$ found by the best fit of $M_z(\alpha)$ with the Stoner–Wohlfarth theory is equal to 0.89, 0.91, 0.92, and 0.91×10^6 erg cm^{-3} for the four cases.

crease and still uses $M_z = M_{\rm rem}\cos\theta_m$ to calculate θ_m, one would get a θ_m which is smaller than the real angle between the magnetization vector and the $+Z$ axis, and hence, obtain a $\langle K_1\rangle$ which is larger than the actual anisotropy constant.

In summary, the film with easy axes oriented differently from patch to patch and with weak exchange on the patch borders has the following properties. In the case of an in-plane applied field, M_x first increases linearly with the external field. In this linear regime every patch moves continuously with the external field. As the field is increased to a certain value, which can be estimated from the statistical Stoner–Wohlfarth theory (see Appendix C), the jump of magnetization vector in some patches occurs and the film begins to be demagnetized. The jump increases M_x but decreases M_z discontinuously, leading to a steeper slope in the $M_x - H_x$ and $M_z - H_x$ curves. After the jump the $M - H$ curve becomes irreversible. For even larger H_x, the jumped patches begin to align towards the applied field, leading to cascades in M_z. When an external field is applied in the $-Z$ direction, the patch with the anisotropy axis farthest away from Z will reverse at first. It then serves as a nucleation center and expands to the whole film, so that the hysteresis loop has a very high squareness. Therefore, the patch character can manifest itself strongly in the in-plane $M - H$ curves, but weakly on the perpendicular hysteresis loop, except that it reduces the critical nucleation field. In the case of rotating field, the measured $\langle K_1\rangle$ is a better representative than that measured with an in-plane field, especially when the rotating field has a large magnitude.

IV. PATCHY FILM WITH RANDOM ANISOTROPY CONSTANT

In this section we study a film where all the patches have perpendicular easy axes, but the values of K_1 are different from patch to patch. As will be seen, the $M_x - H_x$ curve in this film shows a steeper slope for small H_x and the coercivity H_c is smaller than the average anisotropy field, both are common features of many magnetic materials.

The film has a thickness of $h = 500$ Å and a saturation magnetization of $M_s = 100$ emu cm^{-3}. It contains 91 patches of random shapes and sizes, with an average dimension of 250 Å. The exchange stiffness constant $A_x = 10^{-7}$ erg cm^{-1} within the patches and $A_x = 0.4\times10^{-7}$ erg cm^{-1} on all the patch borders. The easy axes are randomly oriented from site to site on the original hexagonal lattice within a 45° cone, but the effective easy axis of each patch is still perpendicular to the film plane, as was explained at the beginning of Sec. III. The anisotropy constant is set randomly from patch to patch, following a truncated Lorentzian distribution of probability given by

$$\rho(K_1) = \frac{1}{\Gamma\left[\arctan\dfrac{K_{\max}-K_c}{\Gamma} - \arctan\dfrac{K_{\min}-K_c}{\Gamma}\right]\left[1+\left(\dfrac{K_1-K_c}{\Gamma}\right)^2\right]}, \quad \text{for } K_{\min}\leqslant K_1\leqslant K_{\max}. \tag{3}$$

This Lorentzian is peaked at K_c, truncated at $K_{\min}$ and $K_{\max}$ [i.e., $\rho(K_1) = 0$ for K_1 outside $(K_{\min}, K_{\max})$], and has a half-height-width of Γ. In the present case we have used $K_c = 10^6$ erg cm^{-3}, $K_{\min} = 2\times10^5$ erg cm^{-3}, $K_{\max} = 1.8\times10^6$ erg cm^{-3}, and $\Gamma = 10^6$ erg cm^{-3}. The corresponding smallest $H_{\rm ani} = 2K_1/M_s$ is 4 kOe and the largest $H_{\rm ani}$ is 35 kOe.

We applied, respectively, an in-plane field, a perpendicular field, and a rotating field to the film. In the former two cases the applied field strength is increased from zero at a rate of 100 Oe ns^{-1}. In the third case we keep the amplitude of the field constant and rotate the field vector at a rate of 10° ns^{-1}.

Figure 13 shows the magnetization states under the in-plane field H_x. The remnant state has $M_z \simeq 0.999M_s$, indicating that each patch has a perpendicular easy axis. In other words, the site-to-site randomness of easy axes is averaged out due to the strong exchange coupling. Thus the anisotropy of the patches differs only in values. The effective anisotropy field H_k in the patch of the lowest value of $H_{\rm ani} = 4$ kOe is equal to $H_k = 0.727H_{\rm ani} - 4\pi M_s = 1.7$ kOe, where the factor 0.727 is derived in Appendix A. Similarly, in the patch of the strongest $H_{\rm ani} = 35$ kOE, we have $H_k = 24.2$ kOe. If the patches are totally disconnected, we expect that each patch would move independently and the one of the lowest H_k would lie entirely in the plane of the film as H_x is increased to about 1.7 kOe, according to the Stoner–Wohlfarth theory. However, from the snapshots of the magnetization states in the simulation, we see that this happens at a field strength of 4 kOe. Figure 13(a) shows the state for $H_x = 4.4$ kOe. This increase is caused by the interaction with the neighboring patches of higher $H_{\rm ani}$. Figure 13(b) and(c) shows the magnetization state for $H_x = 10.6$ and 17.0 kOe, respectively. There we see that the patches falling into the film plane in Fig. 13(a) also bring some neighboring patches moving toward the plane. Therefore, the patches that at the earliest move toward the film plane serve as a nucleation center, which grows with the increasing field. At about $H_x = 20$ kOe, all the magnetization vectors fall in the film plane. The growth of an in-plane domain did not occur in the patchy film with random easy axes discussed in Sec. III. Apparently, the random easy axes produce forces in different directions and make the wall motion harder.

Figure 14 shows M, M_x, and M_z as functions of H_x. In the weak field regime the magnetization vectors turn coherently from the $+Z$ direction to $+X$ direction, and the $M_x - H_x$ curve is a straight line, as predicted by the Stoner–Wohlfarth theory. The movements of the magnetization vectors become apparently incoherent at about $H_x = 4$ kOe, which exceeds the effective H_k of some patches as manifested in Fig. 13(a). The incoherence is also marked by the dip in M. Since the magnetization vectors that already fall in the film plane will not increase their

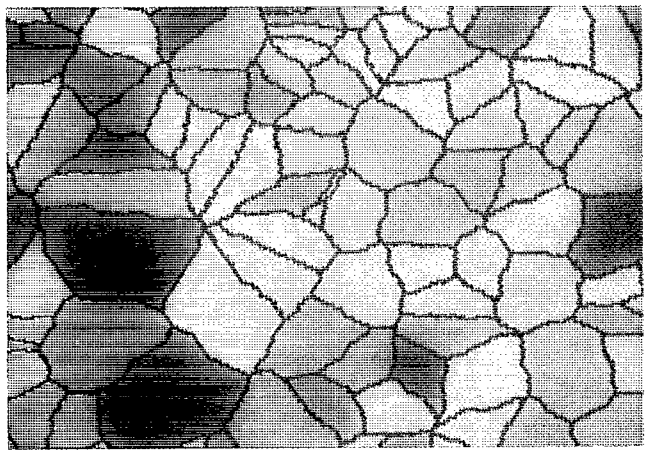

(a)

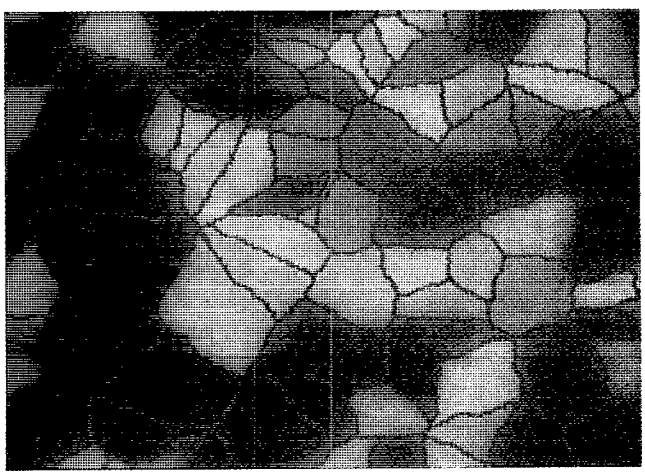

(b)

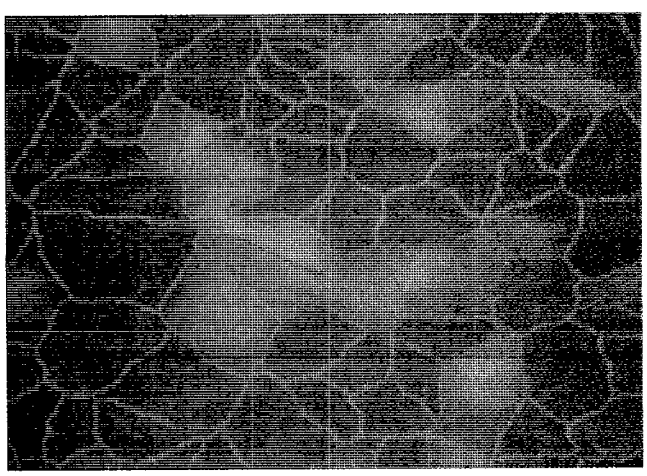

(c)

FIG. 13. Magnetization state under in-plane applied field H_x for the patchy film described in Sec. IV. The film is initially saturated in the $+Z$ direction. (a) The magnetization state at $H_x = 4.4$ kOe. The magnetization vectors in patches with smaller K_1 fall in the plane of the film; see the deeper red patches. (b) The state at $H_x = 10.6$ kOe. (c) The state at $H_x = 17.0$ kOe. We see that the in-plane domains are connected to each other.

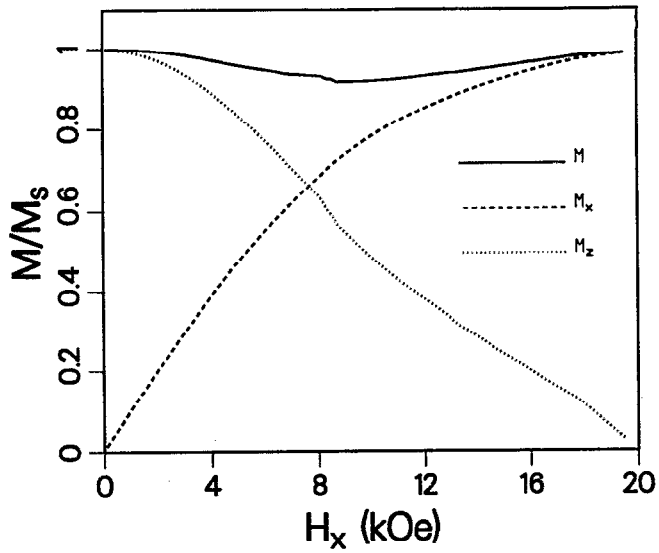

FIG. 14. In-plane $M - H$ curves for the patchy film described in Sec. IV. The $M_x - H_x$ curve shows a common slope observed in many magneto-optical thin films. The best fit of the $M_z - H_x$ curves with the Stoner–Wohlfarth theory gives $\langle K_1 \rangle = 0.55 \times 10^6$ erg cm^{-3}.

X components, the slope of the $M_x - H_x$ curve becomes smaller. This change of slope is a commonly observed feature of many $M_x - H_x$ curves. The best fit of the $M_z - H_x$ curve in the range of $0 \leqslant H_x \leqslant 3$ kOe (the angle between the magnetization vector **M** and $+Z$ is smaller than 20°) with the Stoner–Wohlfarth theory gives $\langle K_1 \rangle = 0.55 \times 10^6$ erg cm^{-3}, which corresponds to an average H_k of 9.7 kOe.

When a perpendicular magnetic field is applied in the $-Z$ direction, the film shows a simple behavior. Nothing changes before the field reaches the critical value of about $H_z = -4.3$ kOe. Figure 15(a) shows the magnetization state at $H_z = -4.4$ kOe, at which a reversed domain appears. This domain expands quickly until the whole film is reversed; see Fig. 15(b). Therefore, the perpendicular hysteresis loop has a sharp squareness at the critical field; see Fig. 16. Here we see that the nucleation coercive field H_c (i.e., the critical field of reversal) is determined by a patch of the smallest effective anisotropy field (around 4.4 kOe), and is smaller than the average $H_k = 9.7$ kOe of the film.

Now we consider the case of rotating the external field. We start from the saturated state. In the first run we let $H_{ext} = 5$ kOe and let the field rotate from $+Z$ to the $-Z$ direction in the X-Z plane. Figure 17(a) is the magnetization state for $\alpha = 90°$ (i.e., the external field is along $+X$), in which several in-plane domains appear. Figure 17(b) shows the state for $\alpha = 110°$, where a lot of patches which are connected to the in-plane patches in Fig. 17(a) are reversed because the field has a large enough $-Z$ component. This domain expands quickly to the whole film as the field is further rotated to $\alpha = 120°$ (not shown). This expansion of domain causes a sharp drop in the $M_z(\alpha)$ curve, as can be seen in Fig. 18(a). We also did the simulations for $H_{ext} = 10$ and 15 kOe. The M, M_x, and M_z as functions of the field angle α for $H_{ext} = 5$, 10, and 15 kOe are plotted in Fig. 18. The different depths of the dip in the

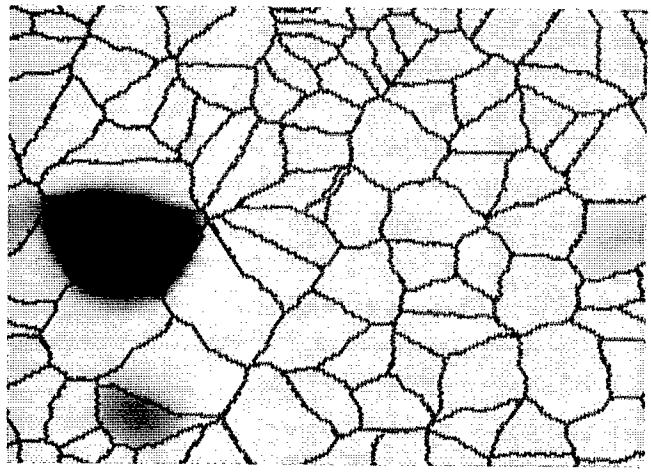

(a)

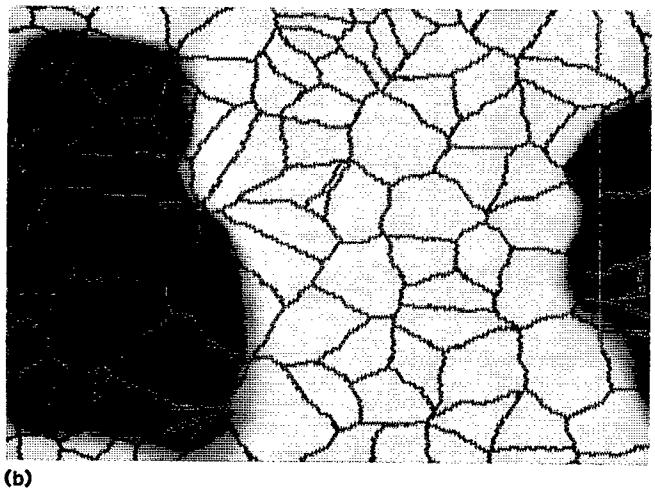

(b)

FIG. 15. The magnetization state under perpendicular applied field H_z for the patchy film described in Sec. IV. The lattice is initially saturated in the $+Z$ direction. (a) A domain is formed at $H_z = -4.4$ kOe. (b) The domain expands quickly to the whole film, so that the hysteresis loop is very sharp at the critical point.

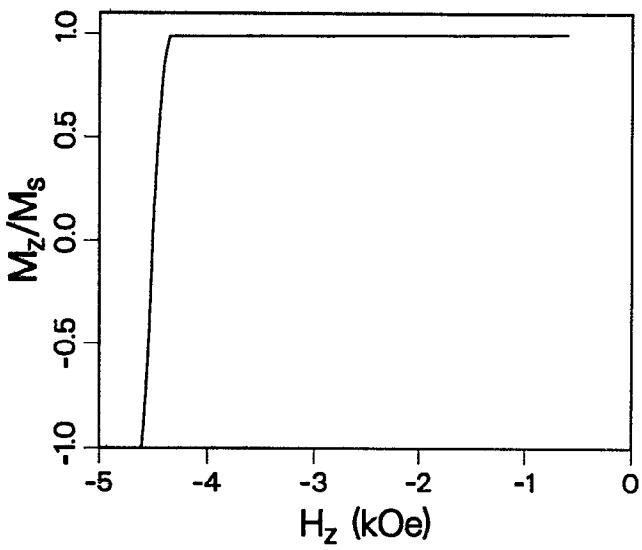

FIG. 16. Perpendicular hysteresis loop for the patchy film described in Sec. IV. The hysteresis loop shows a high squareness.

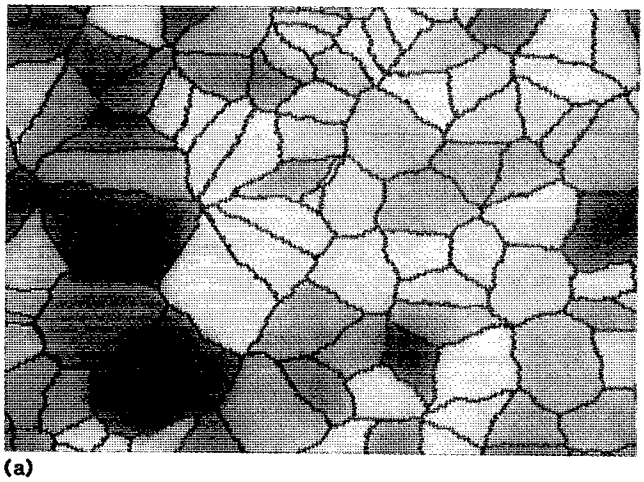

(a)

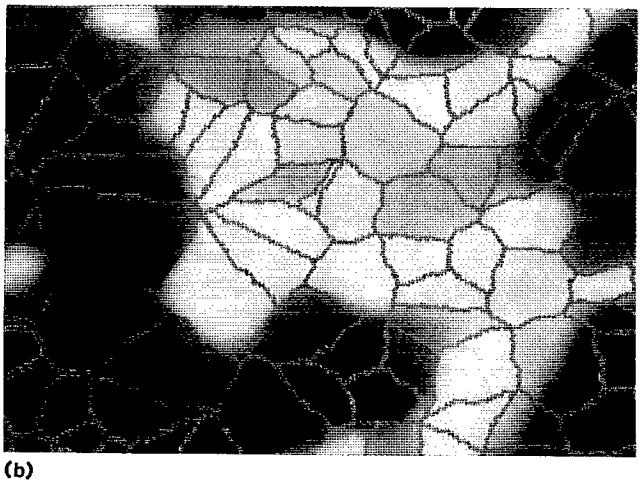

(b)

FIG. 17. Magnetization states for the patchy film described in Sec. IV under rotating field with $H_{ext} = 5$ kOe. (a) Several patches follow the rotating field and fall in the film plane at $\alpha = 90°$. (b) Many patches are reversed as the field is rotated to $\alpha = 110°$, most of which are connected with the first reversed patch. The function $M_z(\alpha)$ at this point shows a sharp drop.

function $M(\alpha)$ show that the magnetization vectors move more coherently for stronger field. The reason is that the randomness of the anisotropy constants which tends to cause the incoherence is suppressed by the strong field. The best fit between the $M_z(\alpha)$ curve shown in Fig. 18 and the Stoner–Wohlfarth theory for $0 \leqslant \theta_m \leqslant 15°$ gives $\langle K_1 \rangle = 0.56$, 0.60, and 0.62×10^6 erg cm^{-3} for $H_{ext} = 5$, 10, and 15 kOe, respectively.

In summary, the patchy film whose patches have perpendicular easy axes but different anisotropy constants has the following properties. In the case of applying an in-plane field, the $M_x - H_x$ and $M_z - H_x$ curves change slopes when H_x exceeds the effective anisotropy fields of some patches. For even larger H_x the $M_x - H_x$ curve becomes flatter, since these patches can no longer contribute to M_x. In the case of applying a perpendicular field, the film shows a hysteresis loop of high squareness at the coercivity H_c, which corresponds to the smallest effective H_k of the patches. $\langle K_1 \rangle$ obtained in the case of rotating field depends

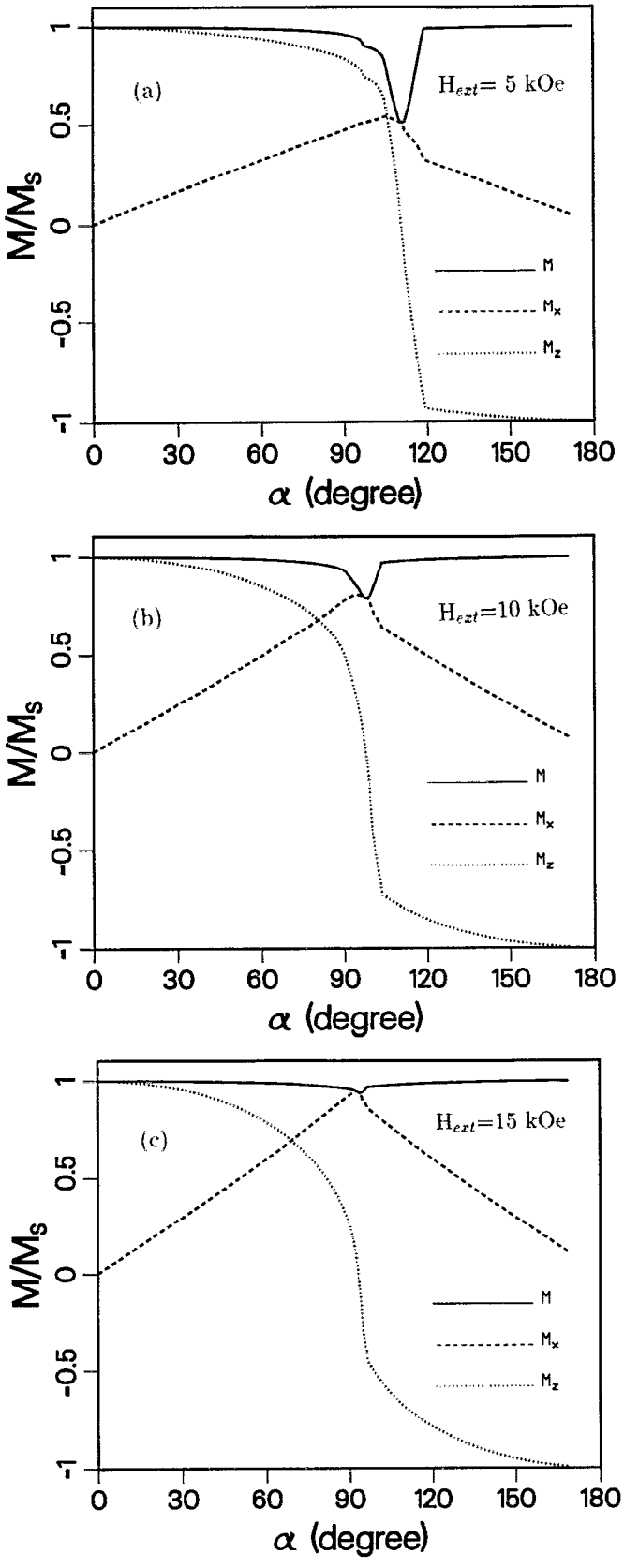

FIG. 18. M, M_x and M_z as functions of the field angle α for different amplitude H_{ext} for the patchy film described in Sec. IV. (a) H_{ext} = 5 kOe. (b) H_{ext} = 10 kOe. (c) H_{ext} = 15 kOe. $\langle K_1 \rangle$ found by the best fit of $M_z(\alpha)$ with the Stoner–Wohlfarth theory is equal to 0.56, 0.60, and 0.62×10^6 erg cm^{-3} for (a)–(c), respectively.

on the field strength: The stronger the field, the bigger the $\langle K_1 \rangle$.

V. CONCLUDING REMARKS AND DISCUSSIONS

We have studied four different patchy films which show a wide variety of magnetic phenomena. The shapes of $M - H$ curves and hysteresis loops depend on the assumed patchy structures, for example, the drop in $M_z - H_x$ curve can be caused by the randomness in easy-axis orientations and the slope change in $M_x - H_x$ curve by the dispersion of the anisotropy constants. The details of the features of each patchy film have been summarized at the end of the sections. In addition to those features that are closely related to a particular patchy film, the following general conclusions may be drawn from these dynamic simulations. (i) The spatial dimension of the inhomogeneities of anisotropy must be large enough to cause incoherent and irreversible magnetic processes. The critical dimension can be estimated as follows. Consider a circular patch of radius r and height h (the film thickness). The anisotropy energy of the cylinder is equal to $\pi r^2 h K_1$. The exchange energy on the cylindrical surface is equal to the number of atoms on the surface times the exchange energy per pair of atoms. The number of atoms on the surface is approximately equal to $2\pi rh/d^2$, where d is the atomic diameter, and the exchange energy per pair atoms is approximately equal to dA_x. Therefore, the exchange energy on the surface is about $2\pi rhA_x/d$. The patch can show its anisotropy only if the anisotropy energy is comparable to or larger than the exchange energy. This requires that $r \geqslant 2A_x/dK_1$. For typical values of $A_x = 10^7$ erg cm^{-1}, $K_1 = 10^6$ erg cm^{-3}, and $d = 4$ Å, it requires $r \geqslant 500$ Å. In reality, the surface of the patch (the cylindrical surface) could be the gap between two columnar structures and the actual exchange stiffness constant A_x could be well below its nominal value. Therefore, the critical patch size could be smaller. (ii) In the presence of patches or inhomogeneities, where the patch borders may even have weak (but nonzero) exchange stiffness constant, the perpendicular hysteresis loops still have sharp squareness. In contrast to this, the in-plane $M - H$ curves are more sensitive to the patch structures. The reason is that the domain wall is hard to move under in-plane applied fields. We may thus conclude that the in-plane $M - H$ curves contain more information about nanoscale structures. (iii) The amplitude of the average magnetization is not always a constant. It can vary within a few percent with the applied field strength, even though the motion of the dipoles seems to be coherent. Neglecting this change can introduce errors in measuring the anisotropy constant.

Although there is little direct information available about patches in magneto-optical thin films, the various incoherent movements of magnetization, the different kinds of irreversible magnetic reversals, and the deviations of the observed $M - H$ curves and hysteresis loops from the Stoner–Wohlfarth theory strongly suggest that there are certain inhomogeneities in magneto-optical thin films. The idea of patchy film presents a model for describing the inhomogeneities. At this stage, the large-scale computer simulations become the only tool to single out each specific mechanism for the observed discrepancies which are unexpected in the framework of uniform and homogeneous

magnetic structure and the coherent rotation theory of Stoner and Wohlfarth.

ACKNOWLEDGMENTS

We thank Roger Hajjar and Te-ho Wu for many helpful discussions. This work has been supported by the Optical Data Storage Center at the University of Arizona.

APPENDIX A: $\langle K_1 \rangle$ FOR LATTICE WITH RANDOM EASY AXES

In the following, we assume that all the sites of the lattice have the same anisotropy constant K_1, but the easy axes are oriented randomly. The probability density for an easy axis to orient in the (θ_a,ϕ_a) direction is given by $\rho(\theta_a,\phi_a)$, where θ_a and ϕ_a have been defined in Sec. I. The probability density satisfies the normalization condition

$$\int_0^{\pi}\int_0^{2\pi} \rho(\theta_a,\phi_a)\sin\theta_a \, d\theta_a \, d\phi_a = 1 . \tag{A1}$$

The problem we will solve is the following: If all the dipoles are parallel aligned due to the exchange coupling, what is the macroscopic anisotropy?

Denote the unit vector along the magnetization direction by $\mathbf{e}_m = \sin\theta_m \cos\phi_m \mathbf{e}_x + \sin\theta_m \sin\phi_m \mathbf{e}_y + \cos\theta_m \mathbf{e}_z$ (see Fig. 19) and the angle between the easy axis at a given site and the magnetization vector by θ_{a-m}. The anisotropy energy density at this site is then given by

$$E_{\text{ani}} = K_1 \sin^2\theta_{a-m} . \tag{A2}$$

Since $\sin^2\theta_{a-m} = 1 - (\mathbf{e}_m \cdot \mathbf{e}_a)^2$, where $\mathbf{e}_a$ is the unit vector along the easy axis direction as introduced in Sec. I, the average anisotropy energy density is

$$\langle E_{\text{ani}} \rangle = K_1 \int_0^{\pi}\int_0^{2\pi} [1 - (\mathbf{e}_m \cdot \mathbf{e}_a)^2] \times \rho(\theta_a,\phi_a)\sin\theta_a \, d\theta_a \, d\phi_a . \tag{A3}$$

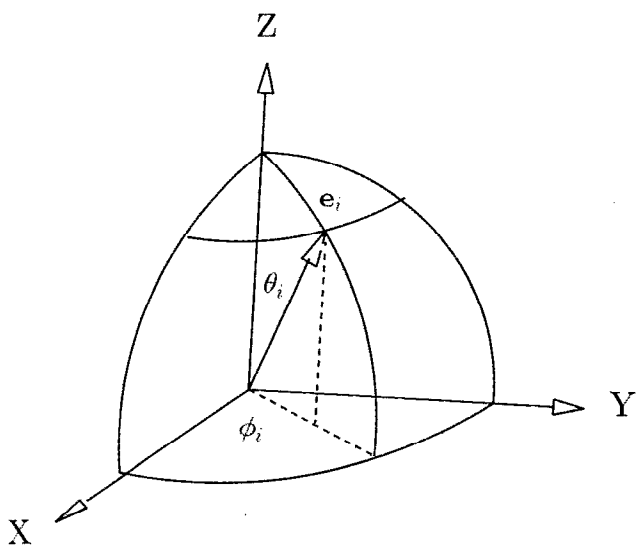

FIG. 19. Definitions of the spherical angles (θ_i,ϕ_i), where $\mathbf{e}_i$ with $i = a, m$ denotes the unit vector along the easy axis and the magnetization direction, respectively. The X-Y plane is the film's plane.

Now we assume that $\rho(\theta_a,\phi_a)$ does not depend on the azimuthal angle ϕ_a, i.e., we assume that the local anisotropy axes are oriented symmetrically about the film's normal direction. But, to remind that ρ is a probability density with respect to the solid angle, we still symbolically write ϕ_a as a variable. Under this assumption, the integration over ϕ_a can be carried out and we obtain

$$\langle E_{\text{ani}} \rangle = \pi K_1 \sin^2\theta_m \int_0^{\pi} (3\cos^2\theta_a - 1) \times \rho(\theta_a,\phi_a)\sin\theta_a \, d\theta_a , \tag{A4}$$

where we have neglected all the terms which are independent of θ_m. Thus the average anisotropy constant is

$$\langle K_1 \rangle = \pi K_1 \int_0^{\pi} (3\cos^2\theta_a - 1)\rho(\theta_a,\phi_a)\sin\theta_a \, d\theta_a . \tag{A5}$$

Now we apply Eq. (A5) to the situation described in Sec. I, where we assumed that θ_a has an equal probability in $(0,\Theta_c)$, where Θ_c is defined as the cone angle, and, *independently*, ϕ_a has an equal probability in $(0,2\pi)$. This probability density distribution is given by

$$\rho(\theta_a,\phi_a) = (2\pi\Theta_c \sin\theta_a)^{-1}, \quad \text{for} \quad \theta_a \in (0,\Theta_c) , \tag{A6}$$

and outside $(0,\Theta_c)$ the probability density is equal to zero. It is easy to check that Eq. (A6) satisfies the normalization condition Eq. (A1) and leads to equal probability for each equal interval of θ_a. Inserting Eq. (A6) in Eq. (A5), we find

$$\langle K_1 \rangle = \frac{K_1}{2\Theta_c} \int_0^{\Theta_c} (3\cos^2\theta_a - 1) d\theta_a = K_1 \left[\frac{1}{4} + \frac{3}{8\Theta_c} \sin(2\Theta_c) \right] . \tag{A7}$$

This equation shows that the average anisotropy axis is perpendicular to the film plane. For $\Theta_c = 45°$, we have $\langle K_1 \rangle = 0.727 K_1$.

It should be emphasized that Eq. (A7) is valid when all the dipoles are perfectly aligned in the same direction. This assumption holds very well for lattice with site to site randomness, as is the case in Secs. I, II, and IV, because for each site the exchange energy usually is much stronger than the anisotropy energy. However, in the case of Sec. III, this assumption does not hold, because each patch has a different anisotropy axis and the exchange coupling is not strong enough to align the magnetization vectors in different patches. Therefore, we cannot use Eqs. (A3) or (A7) to calculate the average anisotropy in that case.

APPENDIX B: DEMAGNETIZING FIELD ON A CIRCULAR PATCH

To find out how the demagnetizing field on a patch is related to the size of the patch and the film thickness, we consider a circular patch of radius r and height h, where h is the film thickness. We assume that the magnetization outside the circular path is saturated in the $+Z$ direction. Under this assumption the demagnetizing field on the circular patch can be completely attributed to the bound current circulating on the cylindrical surface of the patch. Accord-

ing to Ref. 17, the surface current density J_s in the Gaussian unit system is given by

$$J_s = cM_s , \tag{B1}$$

where c is the velocity of light and M_s is the saturation magnetization. The current is rotating around the $-Z$ direction. For any point on the axis of the cylinder, which can be specified by θ_1 or θ_2 as defined in Fig. 20, the magnetic field produced by the surface current is[17]

$$\begin{aligned}\mathbf{B} &= -(2\pi J_s/c)(\cos\theta_1 + \cos\theta_2) \\ &= -2\pi M_s(\cos\theta_1 + \cos\theta_2)\mathbf{e}_z .\end{aligned} \tag{B2}$$

The average field over the axis of the cylinder (i.e., over the thickness of the film) is thus given by

$$\langle\mathbf{B}\rangle = -2\pi M_s \frac{1}{h}\int_0^h (\cos\theta_1 + \cos\theta_2)dz\,\mathbf{e}_z . \tag{B3}$$

This integration can be easily carried out and the final result is

$$\langle\mathbf{B}\rangle = -\left[4\pi M_s h/(r+\sqrt{r^2+h^2})\right]\mathbf{e}_z . \tag{B4}$$

This is the average field along the cylinder axis. We take it as an approximation for the average field over all the cylinder. It is easy to check that in the limit $h \gg r$, the field goes to $-4\pi M_s$ and in the limit $h \ll r$, the field goes to zero. Therefore, the smaller the patch and the thicker the film, the stronger the demagnetizing field. Since we have assumed that all the part outside the patch is magnetized in the $+Z$ direction, the result is valid in the case where only a few patches are reversed.

For the patch lattice discussed in Sec. II, where the film thickness is 1000 Å, the saturation magnetization $M_s = 410$ emu cm^{-3}, using 50 Å as the average radius of the patch, then, according to Eq. (B4), the demagnetizing field on an average patch is approximately equal to 4.9 kOe. This field makes the film easily demagnetized and changes the shape of the $M-H$ curves.

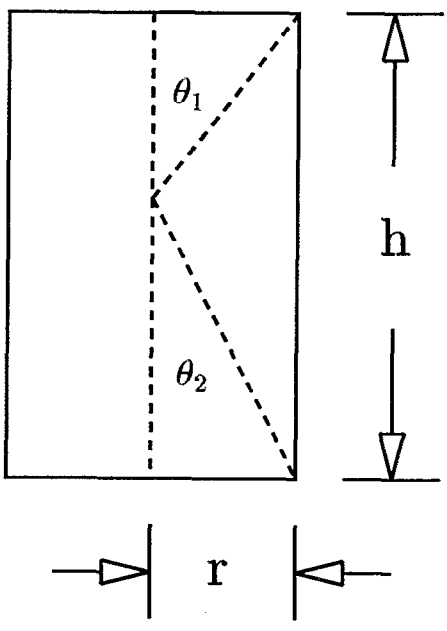

FIG. 20. Definitions of θ_1 and θ_2. The demagnetizing field on the circular patch produced by the rest part of the film which is perpendicularly magnetized in the $+Z$ direction is equivalent to the field produced by a surface current density $J_s = cM_s$ rotating about the $-Z$ direction.

APPENDIX C: STATISTICAL STONER–WOHLFARTH THEORY

Now we want to see how far we can go with the Stoner–Wohlfarth theory if the film is made of patches. We assume that the patches have equal dimensions and are independent from each other; i.e., there is no demagnetizing field and there is no exchange coupling among the patches. For each individual patch, let (θ_a,ϕ_a) be the direction of the anisotropy axis, (θ_m,ϕ_m) the magnetization direction of the patch and (θ_h,ϕ_h) the direction of the external field; i.e., let

$$\mathbf{e}_i = \sin\theta_i\cos\phi_i\mathbf{e}_x + \sin\theta_i\sin\phi_i\mathbf{e}_y + \cos\theta_i\mathbf{e}_z ,$$
$$i = a, m, h. \tag{C1}$$

Then the magnetic energy density for a patch with given $\mathbf{e}_m$, $\mathbf{e}_a$, and $\mathbf{e}_h$ is

$$E = -H_{\rm ext}M_s(\mathbf{e}_h\cdot\mathbf{e}_m) - K_1(\mathbf{e}_m\cdot\mathbf{e}_a)^2 , \tag{C2}$$

where $H_{\rm ext}$ is the strength of the external field. Numerically, it is easy to find out the local equilibrium direction $\mathbf{e}_m$ by finding out the local energy minimum. This equilibrium orientation depends on $\mathbf{e}_a$, $\mathbf{e}_h$, K_1, $H_{\rm ext}$, and the initial direction of the magnetization vector $\mathbf{e}_m^{(0)}$; i.e.

$$\mathbf{e}_m = \mathbf{e}_m(\mathbf{e}_a,\mathbf{e}_h,\mathbf{e}_m^{(0)},K_1,H_{\rm ext}) . \tag{C3}$$

Now we consider two kinds of random anisotropies, corresponding to the patchy films discussed in Secs. III and IV. In the first case we assume that the easy axes are oriented randomly, following a probability distribution density $\rho(\theta_a,\phi_a)$ as given by Eq. (A6) with $\Theta_c = 45°$. Thus, for the ensemble of the patches, the average magnetization is given by

$$\begin{aligned}\mathbf{M} = M_s\int_0^{\pi}\int_0^{2\pi}&\mathbf{e}_m(\mathbf{e}_a,\mathbf{e}_h,\mathbf{e}_m^{(0)},K_1,H_{\rm ext}) \\ &\times\rho(\theta_a,\phi_a)\sin\theta_a\,d\theta_a\,d\phi_a .\end{aligned} \tag{C4}$$

In calculating Eq. (C4) we let $\mathbf{e}_m^{(0)}$ be initially in its corresponding easy axis direction and have a positive Z component. Then, as the field $H_{\rm ext}$ is increased, we let the equilibrium state for one value of $H_{\rm ext}$ to be the initial state for next value of $H_{\rm ext}$. Figure 21(a) and (b) shows the in-plane and perpendicular $M-H$ curves calculated from Eq. (C4). In comparison with the simulation result Fig. 8, we find that the Stoner–Wohlfarth theory produces the main features of the in-plane $M-H$ curve, e.g., the similar slope changes in $M_x - H_x$ and in $M_z - H_x$ curves. Figure 21(a) does not show any cascades in the $M_z - H_x$ curve, because in Eq. (C4) $\rho(\theta_a,\phi_a)$ is a continuous function, while in the patchy lattice it is actually a step function due to lack of sufficient number of patches. The similarities between the simulation result and the present statistical Stoner–Wohlfarth theory shows that, for the lattice with the random easy axes on the patches and with 20% exchange on the patch borders, there is no domain wall motion when an in-plane field is applied to the film. That is, each patch is not

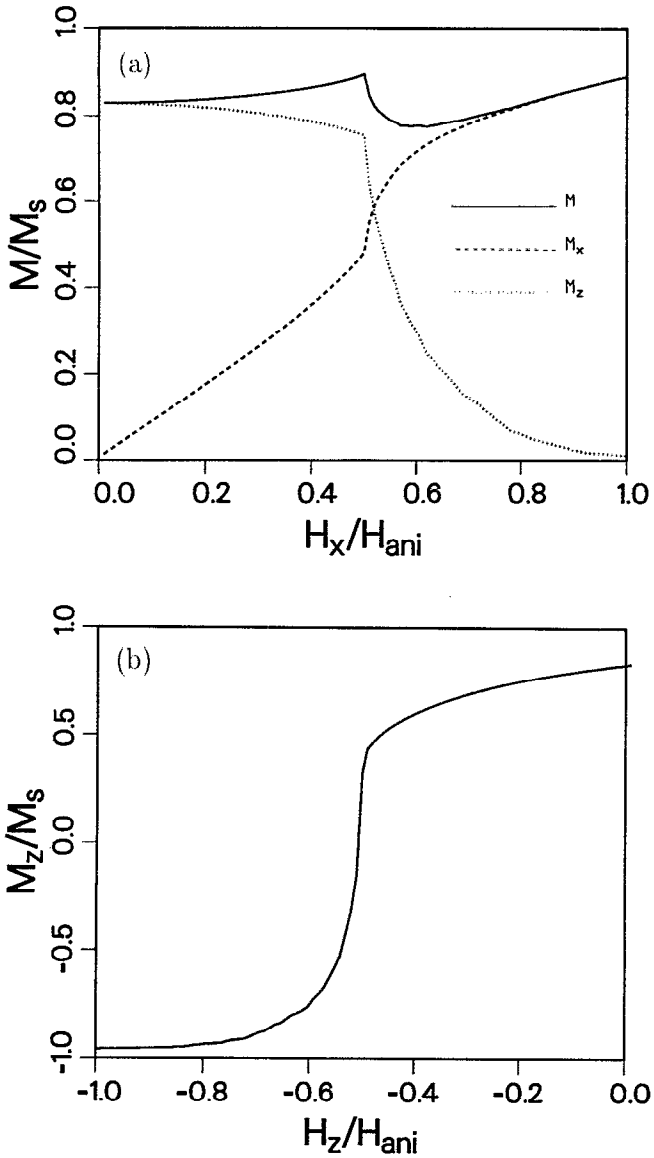

FIG. 21. $M - H$ curves calculated from the statistical Stoner–Wohlfarth theory for an ensemble of independent patches having different easy axes. (a) The in-plane $M - H$ curves. These curves are similar to those shown in Fig. 8. (b) The perpendicular hysteresis loop. This loop is different from Fig. 10. The similarity between (a) and Fig. 8 and the dissimilarity between (b) and Fig. 10 show that the exchange on the patch borders does not cause coherent motion under the in-plane applied field, but it does under the perpendicularly applied field.

too much influenced by other patches. However, the 20% exchange on the patch borders has a strong effect on the perpendicular hysteresis loop, as the difference between Fig. 10 and Fig. 21(b) shows. The dynamic simulation result shows that the exchange on the patch borders is strong enough to let the domain wall move under a perpendicularly applied field. Therefore, Fig. 10 shows a square hysteresis loop.

In the second case we assume that the anisotropy axes of all the patches are in the $+Z$ direction, but with different value of the anisotropy field strength H_{ani} (i.e., anisotropy energy density constant K_1). Figure 22(a) and (b) shows the in-plane and perpendicular $M - H$ curve, respectively, where H_{ani} is the maximum anisotropy field strength. The anisotropy field strengths are distributed homogeneously from $0.5\,H_{ani}$ to H_{ani}. This distribution is not the same as we discussed in Sec. IV. In comparison with Fig. 14, we find that the slope change in the $M_x - H_x$ curve is similar; i.e., it is steep for weak field and becomes flatter for stronger field. The reason is that when the magnetization vector of a patch falls in the plane of the film, this patch will not contribute to the increase of the X component any

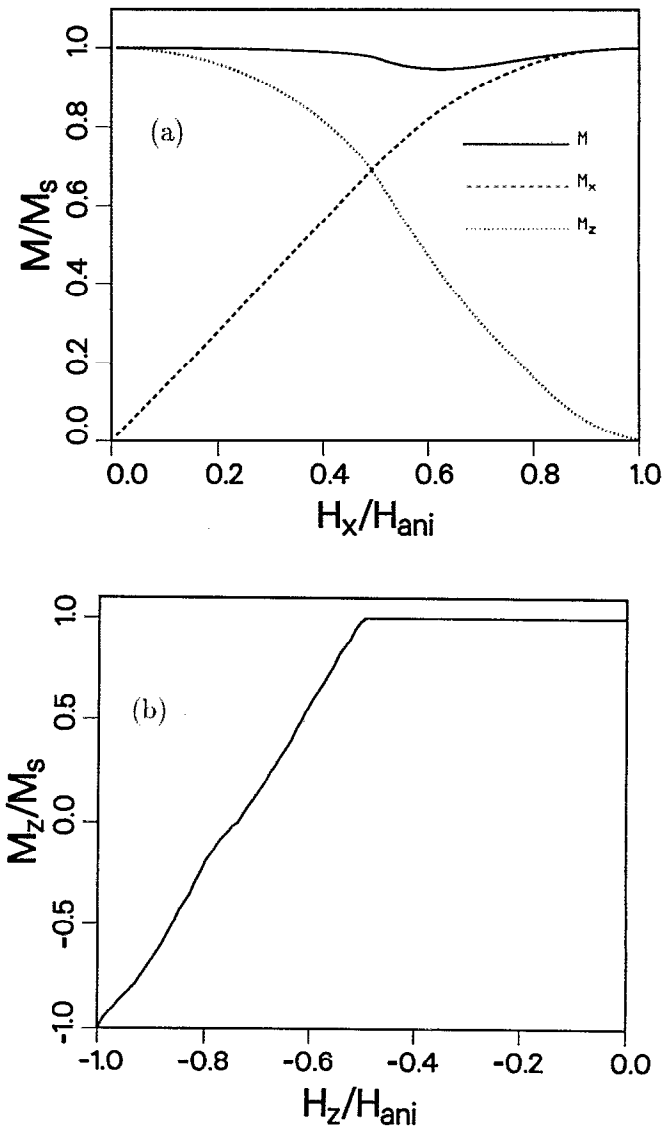

FIG. 22. The $M - H$ curves calculated from the Stoner–Wohlfarth theory for an ensemble of independent patches having different anisotropy constants. (a) The in-plane $M - H$ curves. These curves are similar to those shown in Fig. 14, except that the $M_z - H_x$ curve does not show a sharp drop as in Fig. 14, which is caused by the expansion of the domain of in-plane magnetization vectors. (b) The perpendicular $M - H$ curve. This curve is different from Fig. 16. The 20% exchange on the patch borders in the case of Fig. 16 is strong enough to cause the reversed domain expand to the whole lattice.

more as the in-plane applied field is further increased. Figures 14 and 16 show that there are nucleations for both in-plane applied field and perpendicularly applied field. Therefore, for patches with perpendicular anisotropy axes, the weak exchange on the patch borders may have strong effects, so that the magnetic behavior can neither be described by the Stoner–Wohlfarth theory for a single patch nor by that for an ensemble of independent patches. In this case only the dynamic simulations provide correct results.

REFERENCES

1. H. J. Leamy and A. G. Dirks, J. Appl. Phys. **50**, 2871 (1979).
2. S. Yasugi, S. Honda, M. Ohkoshi, and T. Kusuda, J. Appl. Phys. **52**, 2298 (1981).
3. R. J. Artley, K. Ouchi, and S. Iwasaki, IEEE Trans. Magn. MAG-24, 2335 (1988).
4. L. L. Kazmerski (Ed), *Polycrystalline and Amorphous Thin Films and Devices* (Academic, New York, 1980).
5. Here we only assume the magnetization state of the film is uniform along the film thickness. The effects of the thickness of the film on the various effective magnetic fields, including the demagnetizing field, are still taken into account in the simulations. This assumption should be acceptable for magnetic thin films, which show mostly two-dimensional magnetic patterns.
6. W. von Aulock (Ed.), *Handbook of Microwave Ferrite Materials* (Academic, New York, 1965). According to this handbook, the damping constant $\alpha = |\gamma|\Delta H/2\omega$, where γ is the gyromagnetic ratio, ΔH the resonant line width, and ω the resonant frequency. For various rare-earth garnets and spinal garnets at room temperature, $|\gamma| \simeq 1.76 \times 10^7$ Oe^{-1}s^{-1}, ΔH ranges from 50 to over 1000 Oe, and the representative $\omega = 10$ GHz. In terms of these values, the room temperature α ranges from 0.04–0.88. We shall use $\alpha = 0.5$ throughout this paper. The value of α affects the speed at which the system reaches the steady state, but it should not significantly affect the steady state itself. Therefore, as long as the value of α is uniform for all the lattice site, the value of α should not make much difference for the steady states as we present in this paper. We do not discuss the effects of nonuniformity of α in this paper.
7. M. Mansuripur, J. Appl. Phys. **63**, 5809 (1988).
8. M. Mansuripur and R. Giles, IEEE Trans. Magn. MAG-24, 2326 (1988).
9. M. Mansuripur, J. Appl. Phys. **66**, 3731 (1989).
10. R. Giles and M. Mansuripur, Comput. Phys. **5**, 204 (1991).
11. M. Mansuripur, R. Giles, and G. Patterson, J. Mag. Soc. Japan **15**, 17 (1991).
12. R. A. Hajjar, M. Mansuripur, and H.-P. D. Shieh, J. Appl. Phys. **69**, 7067 (1991).
13. E. C. Stoner and E. P. Wohlfarth, Phil. Trans. R. Soc. London Ser. A **240**, 599 (1948).
14. S. Chikazumi and S. H. Charap, *Physics of Magnetism* (Krieger, Malabar, 1964).
15. P. Wolniansky, S. Chase, R. Rosenvold, M. Ruane, and M. Mansuripur, J. Appl. Phys. **60**, 346 (1966).
16. R. A. Hajjar, Te-ho Wu, and M. Mansuripur, submitted to J. Appl. Phys. (1991).
17. J. D. Jackson, *Classical Electrodynamics* (Wiley, New York, 1975), 2nd Ed., Chap. 5.